

**MECHANICAL DESIGN AND MATERIAL
CHARACTERIZATION OF ADDITIVELY MANUFACTURED
Ti6Al4V CONTROL SURFACE FOR AN AERO VEHICLE
USING SELECTIVE LASER MELTING TECHNIQUE**



By

Syed Waqas Ali Shah

(Registration No: 00000361939)

Department of Mechanical Engineering

School of Mechanical & Manufacturing Engineering

National University of Sciences & Technology (NUST)

Islamabad, Pakistan

(2024)

**MECHANICAL DESIGN AND MATERIAL
CHARACTERIZATION OF ADDITIVELY MANUFACTURED
Ti6Al4V CONTROL SURFACE FOR AN AERO VEHICLE
USING SELECTIVE LASER MELTING TECHNIQUE**



By

Syed Waqas Ali Shah

(Registration No: 00000361939)

A thesis submitted to the National University of Sciences and Technology, Islamabad,

in partial fulfillment of the requirements for the degree of

Master of Science in
Mechanical Engineering

Supervisor: Dr. Sadaqat Ali

School of Mechanical & Manufacturing Engineering
National University of Sciences & Technology (NUST)

Islamabad, Pakistan

(2024)

THESIS ACCEPTANCE CERTIFICATE

Certified that final copy of MS/MPhil thesis written by Regn No. 00000361939 Syed Waqas Ali Shah of School of Mechanical & Manufacturing Engineering (SMME) has been vetted by undersigned, found complete in all respects as per NUST Statues/Regulations, is free of plagiarism, errors, and mistakes and is accepted as partial fulfillment for award of MS/MPhil degree. It is further certified that necessary amendments as pointed out by GEC members of the scholar have also been incorporated in the said thesis titled. **Mechanical Design and Material Characterization of additively manufactured Ti6Al4V control surface for an aero vehicle using Selective Laser Melting Technique**

Signature:



Name (Supervisor): Sadaqat Ali

Date: 19 - Jul - 2024

Signature (HOD):



Date: 19 - Jul - 2024

Signature (DEAN):



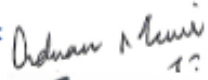
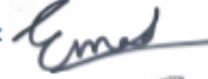
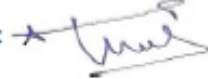
Date: 19 - Jul - 2024



National University of Sciences & Technology (NUST)
MASTER'S THESIS WORK

We hereby recommend that the dissertation prepared under our supervision by: Syed Waqas Ali Shah (00000361939)
Titled: Mechanical Design and Material Characterization of additively manufactured Ti6Al4V control surface for an aero vehicle using Selective Laser Melting Technique be accepted in partial fulfillment of the requirements for the award of MS in Mechanical Engineering degree.

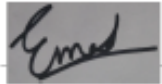
Examination Committee Members

- | | | |
|----|----------------------|--|
| 1. | Name: Adnan Munir | Signature:  |
| 2. | Name: Emad Ud Din | Signature:  |
| 3. | Name: Aamir Mubashar | Signature:  |

Supervisor: Sadaqat Ali

Signature: 

Date: 19 - Jul - 2024



Head of Department

19 - Jul - 2024

Date

COUNTERSIGNED

19 - Jul - 2024

Date



Dean/Principal

CERTIFICATE OF APPROVAL

This is to certify that the research work presented in this thesis, entitled “**Mechanical Design and Material characterization of additively manufactured Ti6Al4V control surface for an aero vehicle using selective laser melting technique**” was conducted by **Mr. Syed Waqas Ali Shah** under the supervision of **Dr. Sadaqat Ali**.

No part of this thesis has been submitted anywhere else for any other degree. This thesis is submitted to the Department of Mechanical Engineering in partial fulfillment of the requirements for the degree of Master of Science in Field of Mechanical Engineering.

Department of Mechanical Engineering, National University of Sciences and Technology, Islamabad.

Student Name: Syed Waqas Ali Shah

Signature:  _____

Examination Committee:

a) GEC Member 1: Emad Ud Din

Signature:  _____

b) GEC Member 2: Aamir Mubashar

Signature:  _____

Supervisor Name: Dr. Sadaqat Ali

Signature:  _____

Name of Dean/HOD: Dr. Emad Ud Din

Signature:  _____

AUTHOR'S DECLARATION

I Syed Waqas Ali Shah hereby state that my MS thesis titled “Mechanical Design and Material characterization of additively manufactured Ti6Al4V control surface for an aero vehicle using selective laser melting technique.” is my own work and has not been submitted previously by me for taking any degree from National University of Sciences and Technology, Islamabad or anywhere else in the country/ world.

At any time if my statement is found to be incorrect even after I graduate, the university has the right to withdraw my MS degree.

Name of Student: Syed Waqas Ali Shah

Date: 19-July-2024

PLAGIARISM UNDERTAKING

I solemnly declare that research work presented in the thesis titled “Mechanical Design and Material characterization of additively manufactured Ti6Al4V control surface for an aero vehicle using selective laser melting technique.” is solely my research work with no significant contribution from any other person. Small contribution/ help wherever taken has been duly acknowledged and that complete thesis has been written by me.

I understand the zero tolerance policy of the HEC and National University of Sciences and Technology (NUST), Islamabad towards plagiarism. Therefore, I as an author of the above titled thesis declare that no portion of my thesis has been plagiarized and any material used as reference is properly referred/cited.

I undertake that if I am found guilty of any formal plagiarism in the above titled thesis even after award of MS degree, the University reserves the rights to withdraw/revoke my MS degree and that HEC and NUST, Islamabad has the right to publish my name on the HEC/University website on which names of students are placed who submitted plagiarized thesis.



Student Signature: _____

Name: _____ Syed Waqas Ali Shah

DEDICATION

Dedicated to my exceptional parents, adored siblings and respected friends for their unending love and support which led to the completion of this thesis.

ACKNOWLEDGEMENTS

I am thankful to my Creator Allah Subhanhu-Watala to have guided me throughout this work at every step and for every new thought which You set up in my mind to improve it. Indeed, I could have done nothing without Your priceless help and guidance. Whosoever helped me throughout the course of my thesis, whether my parents or any other individual, was Your will, so indeed none be worthy of praise but You.

I am profusely thankful to my beloved parents who raised me when I was not capable of walking and continued to support me throughout every department of my life.

I acknowledge and appreciate the guidance and valuable suggestions of Dr. Sadaqat Ali under whose supervision, this study has been completed. I would also like to thank Dr. Aamir Mubashar, and Dr. Emad Ud Din for being on my thesis guidance and evaluation committee and express my special thanks to Dr. Himayatullah for his help. I am also thankful to Mr. Muhammad Saad and Mr. Ahsan Naeem for their support and cooperation.

TABLE OF CONTENTS

ACKNOWLEDGEMENTS	viii
List of Figures.....	xii
List of Tables.....	xiv
ABSTRACT.....	xv
CHAPTER 1: Introduction.....	1
1.1 Background Scope, and Motivation.....	1
1.1.1 Rapid prototyping (RP).....	1
1.1.2 Additive Manufacturing (AM).....	3
1.1.3 Types of Additive Manufacturing	9
1.1.3.1 Liquid-based additive manufacturing	9
1.1.3.2 Solid-based additive manufacturing	9
1.1.3.3 Powder-based additive manufacturing.....	9
1.1.4 Selective laser Melting.....	10
1.1.4.1 Working Principle:.....	10
1.1.4.2 Parameters:	11
1.1.4.3 3D Printing of Ti6Al4V Using Selective Laser Melting Techniques	15
1.1.4.4 Advantages of 3D Printing Ti6Al4V with SLM:.....	16
1.1.4.5 Challenges and Considerations:.....	17
1.1.5 Applications of 3D Printed Ti6Al4V Components:.....	18
1.1.6 Aerospace Industry and AM:	19
1.1.6.1 Aircraft structure.....	19
1.1.6.2 Vertical Control Surface:	20
1.2 Problem statement.....	24

1.3	Purpose and objectives:	24
1.4	Scope:	24
CHAPTER 2: Materials and Method		26
2.1	Design of control surface	27
2.2	Fabrication of samples	29
2.3	Tensile Testing:.....	30
2.4	3 Point bending test:.....	33
2.5	Rockwell Hardness Test:	35
2.6	Thermal Conductivity test by GHFM:	36
2.7	Thermal Coefficient of Expansion test by Dilatometer (DIL-402C):	38
2.8	Specific Heat capacity test by differential scanning calorimeter:	40
2.9	Numerical Simulation Setup:	41
CHAPTER 3: RESULTS		43
3.1	Optimized Control Surface Design:	43
3.2	Fabricated samples by FARSOON machine:	44
3.3	Tensile testing Results:.....	45
3.4	3 Point bending test Results:	47
3.5	Rockwell Hardness Test Result:.....	49
3.6	Thermal conductivity test Results:.....	50
3.7	Thermal coefficient of expansion Test Results:	52
3.8	Specific heat capacity Test Results:	53
3.9	Numerical Simulations:.....	54
3.9.1	Boundary Conditions:	54
3.9.2	Results:.....	54
3.9.2.1	Von-Mises stress:.....	55

3.9.2.2	Total Deformation:	56
3.9.3	Conclusion	57
CHAPTER 4:	DISCUSSION.....	58
4.1	Comparison between Tensile strengths of Ti6Al4v 3D printed Samples and Conventional manufactured Ti6Al4v sheet:	58
4.2	Comparison between thermal conductivity of Ti6Al4v 3D printed Samples and Conventional manufactured Ti6Al4v sheet:	60
4.3	Comparison between coefficient of thermal expansion of Ti6Al4v 3D printed Samples and Conventional manufactured Ti6Al4v sheet.....	62
4.4	Comparison between Specific heat of Ti6Al4v 3D printed Samples and Conventional manufactured Ti6Al4v sheet:	65
CHAPTER 5:	CONCLUSION	70
References		73

LIST OF FIGURES

Figure 1. 1: Product development Cycle.....	2
Figure 1. 2: Increased use of rapid prototyping	3
Figure 1. 3: Classification of additive manufacturing processes.	6
Figure 1. 4: Generic steps in AM process.....	8
Figure 1. 5: Selective Laser Melting Process.....	11
Figure 1. 6: Selective Laser Melting Parameters	13
Figure 1. 7: 3D printed titanium parts: Hip joints, fan blade, rocket tip, titanium lattice component, titanium bracket, surgical spinal implant	16
Figure 1. 8: AM Additive Manufacturing market share	19
Figure 1. 9: Components of fixed-wing aircraft	20
Figure 1. 10: Visualizing the Research Scope and Sequential Stages	25
Figure 2. 1: Research Methodology Flowchart.....	26
Figure 2. 2: Initial Solid Design With leading and trailing sides.....	27
Figure 2. 3: Honeycomb structure	28
Figure 2. 4: Ribbed Structure.....	28
Figure 2. 5: Farsoon FS421M machine for printing of test specimens through SLM	29
Figure 2. 6: samples for testing at room temperature	30
Figure 2. 7: samples for testing at elevated temperatures	31
Figure 2. 8: UTM with furnace for elevated temperature testing	31
Figure 2. 9: Dimensions of tensile testing sample at Room Temperature	32
Figure 2. 10: Dimensions of tensile testing sample at elevated temperatures	32
Figure 2. 11: Dimensions of Fracture toughness sample.....	34
Figure 2. 12: Rockwell hardness tester machine	35
Figure 2. 13: samples for thermal conductivity test.....	36
Figure 2. 14: Guarded heat flow meter	37
Figure 2. 15: Dilatometer (DIL-402C).....	38
Figure 2. 16: Push rod Dilatometer.....	39
Figure 2. 17: sample for DSC test.....	40
Figure 2. 18: Differential Scanning Calorimeter	40
Figure 2. 19: Boundary Conditions.....	42
Figure 3. 1: Stress vs Strain curve for tensile testing sample	45
Figure 3. 2: Fracture of tensile testing sample at room temperature	45
Figure 3. 3: Fracture of tensile testing sample at elevated temperatures	46
Figure 3. 4: load vs deflection curve for tensile testing sample.....	47
Figure 3. 5: Breakage of fracture toughness test sample	48
Figure 3. 6: Thermal conductivity vs Temperature plot	51
Figure 3. 7: CTE vs Temperature Plot	52
Figure 3. 8: Specific heat vs Temperature Plot.....	53
Figure 3. 9: Von-Mises Stress (MPa) in initial solid control Surface.....	55
Figure 3. 10: Von-Mises Stress (MPa) with test properties.....	55
Figure 3. 11: Total Deformation (mm) in initial solid control Surface	56
Figure 3. 12: Total Deformation (mm) with test properties.....	56

Figure 4. 1: Percentage of Room Temperature strength vs Temperature for Ti6Al4V sheet at different Temperature 58
Figure 4. 2: Percent Elongation vs Temperature for Ti6Al4V sheet at different Temperature 59
Figure 4. 3: Thermal Conductivity vs Temperature for Ti6Al4V sheet at different Temperature. 60
Figure 4. 4: CTE vs Temperature for Ti6Al4V sheet at different Temperature 63
Figure 4. 5: Specific heat vs Temperature for Ti6Al4V sheet at different Temperature..... 65

LIST OF TABLES

Table 2.1: Specifications of FARSOON Machine.....	29
Table 2.2: Printing parameters for Printing Samples.....	30
Table 3.1: Properties obtained from Tensile testing samples at elevated temperatures.	46
Table 3.2: comparison of FEA results of initial solid design and final optimized ribbed structure design	57
Table 4.1: Comparison of tensile strength of 3D printed Tested samples of Ti6Al4V and standard properties of Ti6Al4V.....	59
Table 4.2: Comparison of thermal conductivity of 3D printed Tested samples of Ti6Al4V and standard properties of Ti6Al4V sheet.....	61
Table 4.3: Comparison of CTE of 3D printed Tested samples of Ti6Al4V and standard properties of Ti6Al4V sheet.....	63
Table 4.4: Comparison of Specific heat of 3D printed Tested samples of Ti6Al4V and standard properties of Ti6Al4V sheet.....	66
Table 4.5: Comparison of 3D printed Tested Properties of Ti6Al4V and standard properties of Ti6Al4V.....	68

ABSTRACT

The 3D printing of metals from powder is an emerging technology in the field of material and manufacturing producing complex shape light weight geometries directly from design data. Selective laser melting is one of the promising additive manufacturing techniques for providing near net shape, less material waste, short leading time, and low cost. Ti6Al4V serves as a great material of choice for this manufacturing technique and provides an excellent combination of properties in aerospace structures because of lightweight, high strength, corrosion resistance and high service temperatures. The aim of this project is to design and optimize control surface and additively manufactured it from Ti6Al4V alloy using Selective laser melting technique. Also, to characterize the material properties of SLMed printed Ti6Al4V alloy to measure thermal and mechanical properties and their comparison with traditional manufactured products mentioned in MIL-HDBK standard. Samples are printed and tested on UTM to measure yield strength, tensile strength, Young's Modulus and percentage elongation at room temperature and at elevated temperatures up to 600C⁰. The tensile strength dropped by 67% from room temperature to 600C⁰. A 3-point bending test is conducted to measure critical Bending strength, Flexural Modulus, and stress intensity factor. Thermal Conductivity is measured by GHFM up to 300C⁰. coefficient of thermal expansion and specific heat is measured up to 600C⁰ by dilatometer and scanning calorimeter respectively. All these results are compared with traditional manufactured parts concluded that SLMed products can be used for the same strength and application with less cost, material, and time.

Key Words: Additive Manufacturing, Selective Laser Melting Technique, Ti6Al4V alloy, Control surface, Mechanical Testing, Thermal Testing.

CHAPTER 1: INTRODUCTION

This Research work has been presented in two parts. The first part focused on design of control surface for an aero vehicle control surface. The objective of this part is to design and optimize control surface for ease 3D printing by Farsoon FS421M using selective laser melting technique. The second part is related to the testing of 3D printed Ti6Al4V samples and its characterization. The testing includes mechanical testing i.e. tensile, fracture toughness, hardness and thermal testing i.e. thermal conductivity, coefficient of thermal expansion, specific heat.

1.1 Background Scope, and Motivation

1.1.1 *Rapid prototyping (RP)*

A group of technologies which are used for creating the physical models automatically using computer-aided design (CAD) are known as Rapid Prototyping (RP). This is also defined as a set of techniques for quickly fabricating scaled-down models of actual physical parts or of ambled parts using the same CAD data. Designers may quickly produce actual prototypes of their designs using "three-dimensional printers" rather than two-dimensional representations. These types offer a wide range of applications. Aside from design testing, they are fantastic visual assistance for collaborating with co-workers or clients on ideas. An Aerospace Engineer, for example, would place a duplicate aerofoil in a wind tunnel to observe the aerodynamic forces like lift and drag forces [1].

Rapid prototyping, which was established in the early 1980s for making look-alike duplicates and prototype components, was the first method to make a three-dimensional object through the addition of material as layer-by-layer using computer-aided design (CAD). This technological advancement originated to help and assist in the implementation of the engineers' vision. Among the earliest additive manufacturing (AM) technologies was rapid prototyping. It enables the development of printed parts as well as models. Among the primary breakthroughs that this approach has brought to part manufacturing and modelling are the significant reduction in the amount of time and cost and labour required for guidance and proceeding with process as well as the ability to make practically any shape that was previously difficult to machine.

Figure 1 depicts the phases involved in developing a product utilising rapid prototyping. It is clear from this example that developing models faster saves time and allows for the testing of more models. Rapid prototype technologies are being utilised for more than just generating models; with advancements in polymeric materials, it has made it possible to fabricate final and applicable parts for different purposes and requirements. Although initially they were only applicable to broaden the conditions examined in process of modelling or prototyping. This group of technologies are now known by different names, such as 3D printing, but they all stem from fast prototyping [2].

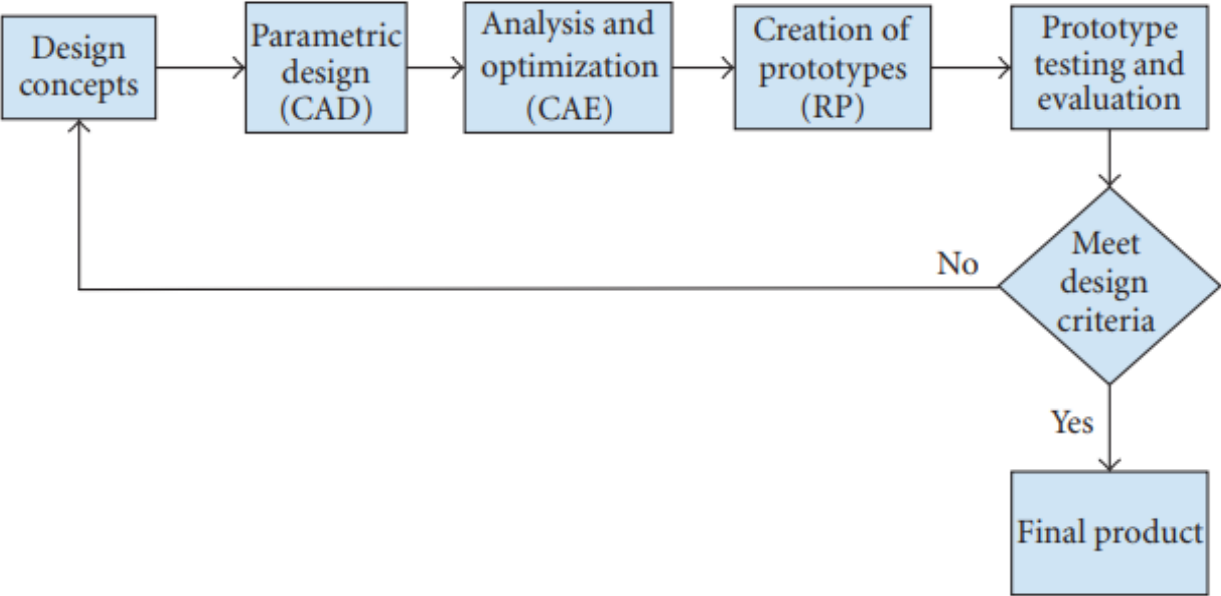


Figure 1. 1: Product development Cycle[3]

The 2010 growth rate was 24.1 percent, according to Wohler's 2011 report. Until 2010, the industry's compound annual growth rate was 26.2 percent. Figure 3 depicts this expansion. Furthermore, additional technologies such CAD, computer-aided manufacturing (CAM), and computer numerical control (CNC) have made quick manufacturing possible. The combination of these three technologies enabled the printing of three-dimensional objects [4].

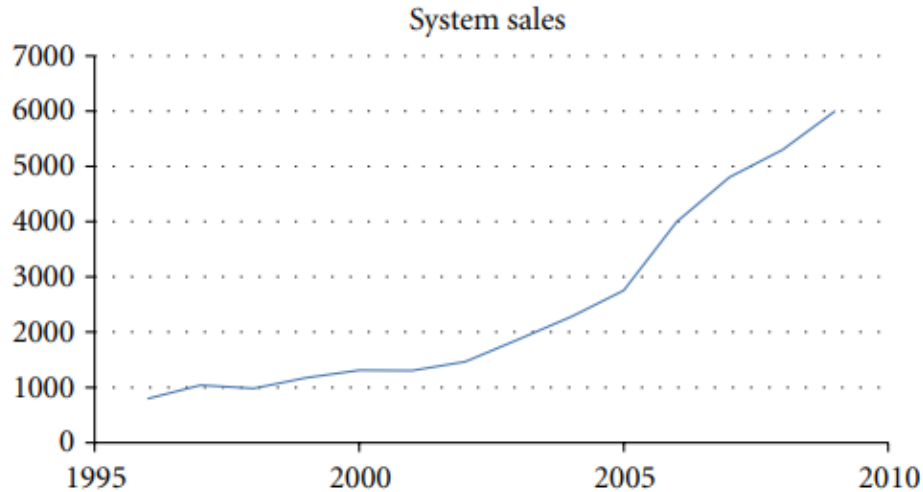


Figure 1. 2: Increased use of rapid prototyping[3]

Rapid prototyping offers following advantages in manufacturing.

- Reducing the time, it takes to build a product and its prototype from a month to weeks and days.
- It is easier to design and exhibit a real tangible model of a future product to customers.
- Although the physical model is easy to rectify, faults in the graphical depiction of the product are possible.
- Tooling and design iteration costs are reduced.
- Product prototypes are less expensive than traditional approaches.

1.1.2 Additive Manufacturing (AM)

3D printing is another term used for additive manufacturing (AM). AM use technique of adding material in layer-by-layer configuration to create a part or prototype. It's not the same as subtractive manufacturing techniques like milling, cutting, drilling, and so on. ASTM describes process of additive manufacturing (AM) as "a technique to manufacture part of assembly from 3D model data, generally in layer-by-layer format,". Synonyms include "additive fabrication," "additive processes," "additive procedures," "additive layer manufacturing," "layer manufacturing," and

"freeform fabrication." Material used in additive manufacturing includes Metals, ceramics, polymers, composites, and biological systems. While additive manufacturing (AM) has been around for at least two decades as a method of material processing, recently it is been used as a significant commercial manufacturing technology. AM can be used to get manufactured parts with extremely detailed and complicated geometries with little post-processing requirements, made from customized materials with almost very low and negligible material waste. This has made it possible to decrease the overall production cost [5].

AM is a tool that gives designers and engineers more freedom and easiness to make changes in the design and geometry of parts. It has also made it possible to make unique and complicated products at low cost and in smaller volumes. One example of the design freedom provided is the ability to redesign conventional assemblies into one whole complicated assembly that can be very difficult and almost impossible to manufacture using other available production procedures. One more motivator for AM technology is its environmental and ecological potential. AM technologies, methodologies and their use are continuously growing. AM process have been extended into many industrial sectors and wings such as automobile industry, medical industry, and aerospace industry, and this fast growth is expected to continue in the coming era [6]. Apart from this AM technology requires lesser tools, a lesser inventory management system. As AM produces a component through layer-by-layer addition of material, this gives the user and industry the freedom of producing lightweight structures. Aside from these benefits, several sustainability benefits are associated with AM, such as shorter supply chains, localized production, and the freedom to alter design and manufacture to order manufacturing [7].

AM differs from rapid prototyping in that it focuses on the production of parts used in different applications and not only prototypes. In recent years AM has made its impact quite bigger and the use of AM processes has steadily increased, and estimates suggest that it might account for more than 5% of the total world market. AM processes also have some challenges like low production, lesser surface finish quality, and mainly the unpredictable nature of the mechanical properties of the printed parts [8]. AM technologies use software and 3D scanners to manufacture parts for different applications in the worldwide market. New modern age factories and manufacturing industries prefer customized production rather than mass productions, resulting in a considerable reduction in time required to manufacture. Additive manufacturing is offering critical

breakthroughs to the modern-age industry. Its use is found in almost all engineering fields, medicinal, scientific, and similar more related domains. AM generates speedy progress to bring the trend to meet the needs of specific customers [9]. AM is very quickly placing itself in one of the most popular technologies around the world, with the ability to completely transform the new era industrial sector. It counts for a new industrial paradigm for changing the way of production and manufacturing, as it rapidly generates a wide range of items made of various materials. Nowadays, AM is even commonly utilized in food printing, such as the printing of personalized pizza, burgers, nourishment, chocolate, cake, and coffee, among other things [10]. Another distinct feature of 3D printing is mass customization or the manufacture of a combination of personalized things in such a way that every component can be unique while reducing the cost due to bulk creation. 3D printing eliminates the additional costs associated with mold creation and tooling for a customized product. As a result, bulk manufacture of many Masses manufacture of numerous different personalized things can be as cost-effective as identical parts. The shift between designs is easy and uniform with no complications and with no extra expense and special extra efforts for preparing is required. Traditional manufacturing processes such as casting are difficult to use and require additional time-consuming equipment and post-processing for complicated structures such as lattice structures. AM offers the ability to mass-produce complex geometries such as lattice structures. Machine design improvements, on the other hand, are required to accommodate advancements in fabrication speed and cost reduction. Furthermore, the high prices and time required in most AM technologies and processes continue to be substantial impediments to mass production[11].

Main elements to enhance the use of AM technology are rapid-prototyping, easiness, and freedom in the printing of huge, complicated structures, the reduction of printing defects, and the enhancement of mechanical properties [12].

The above all and many more advantages of AM over conventional manufacturing processes makes it one of the most preferable and fast-growing manufacturing techniques used in the industry.

There are numerous additive manufacturing procedures available today; They differ in the way layers are deposited to construct things, the working principle, and the materials that may be used. Based on the material used AM has been classified into mainly three categories. These are:

- Liquid-based AM Process
- Powder-based AM Processes
- Solid-based Am Processes

The detailed classification has been categorized below.

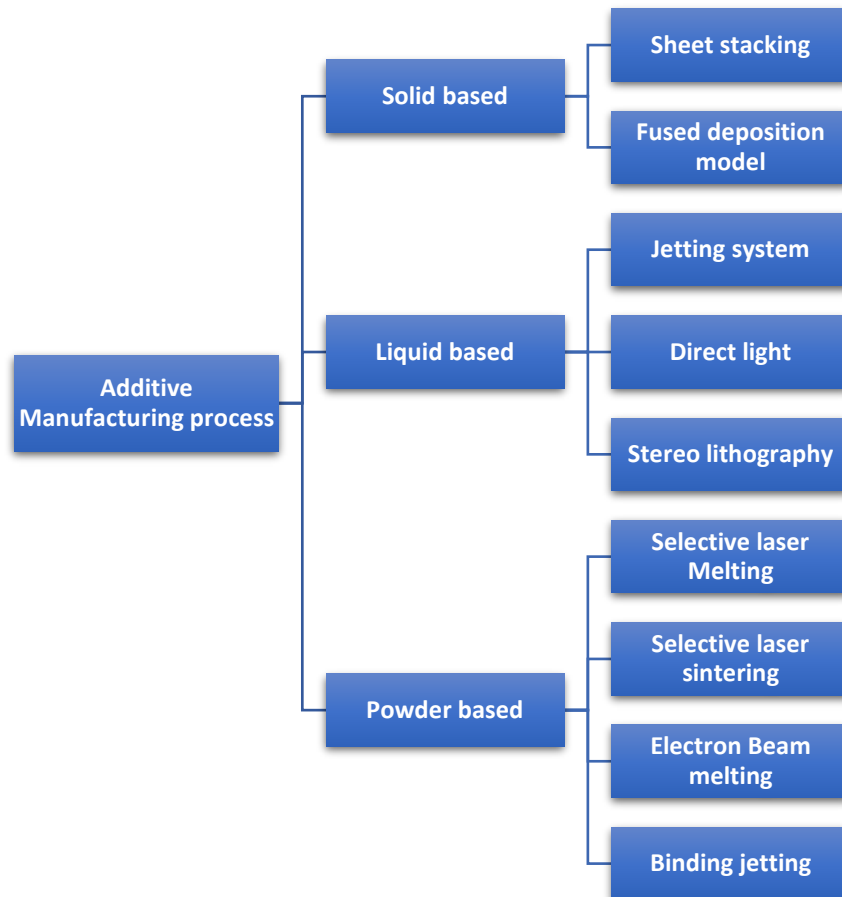


Figure 1. 3: Classification of additive manufacturing processes.

All types of additive manufacturing have their advantages and limitations. All AM techniques involve a range of processes that lead from CAD modelling of geometry to the final printed part. AM is utilized in different ways by different components. Smaller, simpler products sometimes will just require AM for showing prototype and conceptual models, but bigger, more

complicated products with large number of definitions and explanation may use AM at numerous stages and cycles till the final part is printed. In this scenario, AM is favorable because of the complexity of structure that may be produced without the use of tools. To recap, most AM procedures include at least one of the eight phases listed below [13].

Step 1: CAD

All additive manufactured objects always begin with a model developed through software that properly represents the exterior shape and geometrical. About every professional CAD, solid modelling software can be used for this, however, the final file must be a three-dimensional or of a solid surface.

Step 2: Conversion of CAD to STL

Every AM printer requires input file of the part printed in STL file format which is a de facto standard. This STL file can be obtained from every CAD software. This format represents the CAD model's outer closed surface, and it also counts the slices.

Step 3: Manipulation of STL files and transfer to AM machine

The size position and orientation of the part to be printed is confirmed and the proper placement for printing is made sure through manipulation of STL file. For this purpose, the STL file format is given to the AM printer as an input.

Step4: Machine setup

Before the build process, the AM printer must be correctly configured and calibrated. Such settings would apply to construction variables such as material restrictions, energy supply, layer height, timings, and so on.

Step 5: Printing process

The manufacturing process is mostly robotic, and the machine can operate on its own for the most part. At this stage, all that is necessary is a quick assessment of the machine to ensure that no issues like power fluctuations, material shortage or unavailability and some faults in software have arisen.

Step 6: Removal

When the printing of parts is completed and the AM printer stops running, the finished parts are removed safely. This could involve humans interacting with the printer for which safety measures should be observed. Such measures can involve like chamber temperature is suitably lower and that no moving parts are still incomplete or been in process of printing.

Step 7: Post-processing

Some parts need to be post processed after they are printed. This is done sometime to remove the support structures or make it fit for use. As a result, this frequently necessitates time and delicate, skilled individual handling [14].

Following figure 4 shows the general steps and stages used in AM process.

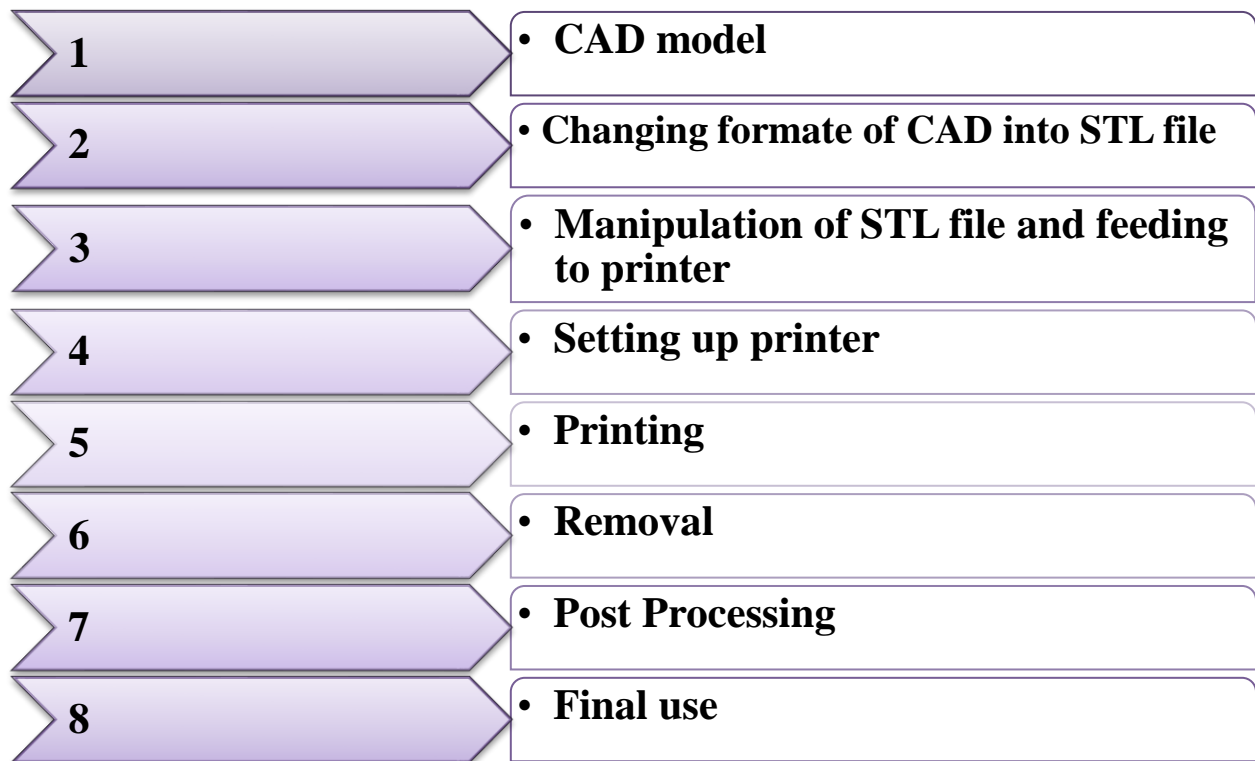


Figure 1. 4: Generic steps in AM process.

1.1.3 Types of Additive Manufacturing

The main three types of AM are defined as

1.1.3.1 Liquid-based additive manufacturing

It appears that liquid polymers are a popular substance. The 3D Systems Stereolithography technique based on liquid photopolymers was the first commercial system. A major portion of today's systems is liquid photopolymer systems rather than liquid polymer systems. Majority of these liquid-based AM printers do the printing process in a vat of photocurable liquid resin, that hardens when exposed to light, typically ultraviolet light. The light solidifies the resin close to the surface, resulting in a fine, solid coating. After the whole layer of the component has been manufactured, a control system lowers the part letting the next layer of resin to be solidified in the same manner till the whole part is formed [15].

1.1.3.2 Solid-based additive manufacturing

Solids are used as the principal medium in solid-based additive manufacturing (AM) systems to build the item or prototype. As such, they differ significantly from liquid-based photo-curing methods. They also differ in that the principal form of solid materials in some systems may be filaments or wires, sheets or rolls in others, and pellets in still others[16].

1.1.3.3 Powder-based additive manufacturing

Powders are often small size particles that have been graded to have a reasonably consistent particle size and shape, as well as a restricted size distribution. The smaller the powder size, the better it is for printing process. Issues managing the distribution and dispersion if the dimensions get too small. Support is not required for powder-based printing systems hence the powders itself act as support for the printing layers. As a result, powder bed-based systems are among the simplest to set up for a basic build. The Powder-based additive manufacturing is further divided into.

- **Selective laser Melting**
- **Selective laser**

- **Electron Beam melting**
- **Binding jetting**

1.1.4 Selective laser Melting

Selective Laser Melting (SLM) is an additive manufacturing process that belongs to the broader category of 3D printing techniques. It offers unique capabilities in producing complex geometries with excellent material properties, making it a popular choice in various industries ranging from aerospace and automotive to healthcare and consumer goods. In this comprehensive overview, we delve into the working principle, parameters, advantages, and disadvantages of the SLM technique[17].

1.1.4.1 Working Principle:

The working principle of SLM involves the selective melting of metal powder layers using a high-powered laser beam. The process begins with the generation of a 3D computer-aided design (CAD) model, which is then sliced into thin layers. These layers typically range from 20 to 100 microns in thickness, depending on the specific application requirements.

1. The SLM machine consists of a build platform, a recoater, and a laser system. Initially, a thin layer of metal powder is spread evenly onto the build platform using the recoater. The recoater ensures a uniform layer thickness, which is crucial for achieving accurate part dimensions.
2. Once the powder layer is in place, the laser system selectively melts the powder according to the cross-sectional shape of the part as defined by the CAD model. The laser beam is precisely controlled using scanning mirrors or galvanometers, allowing for the accurate deposition of energy onto the powder bed. As the laser scans over the powder layer, it raises the temperature above the material's melting point, causing fusion and solidification upon cooling.
3. After completing one layer, the build platform descends by the specified layer thickness, and the recoater applies a new layer of powder. This process is repeated layer by layer until

the entire part is fabricated. Post-processing steps such as heat treatment, machining, and surface finishing may be required to achieve the desired mechanical properties and surface quality.

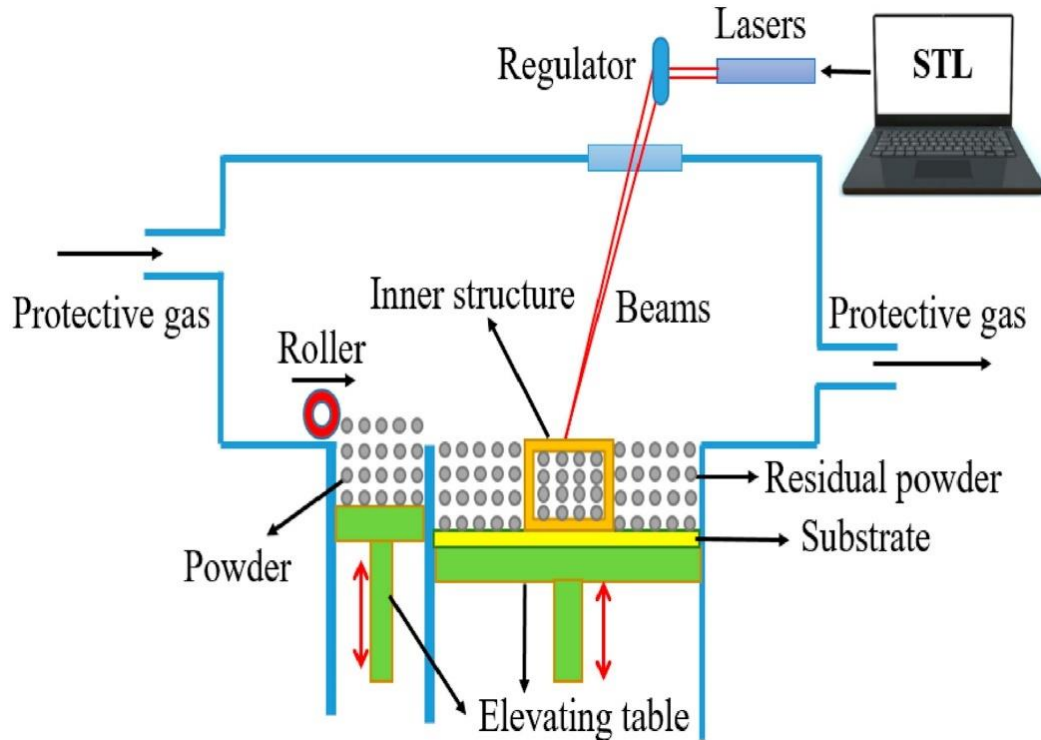


Figure 1. 5: Selective Laser Melting Process[18]

1.1.4.2 Parameters:

Several parameters influence the quality and characteristics of parts produced using the SLM technique:

1. **Laser Power:** The power of the laser beam determines the rate of energy deposition and, consequently, the melting and solidification behavior of the powder. Higher laser powers enable faster build rates but may also lead to increased thermal stresses and distortion.

2. **Scanning Speed:** The speed at which the laser beam moves across the powder bed affects the energy density delivered to the material. Optimal scanning speeds ensure sufficient energy absorption without causing defects such as balling or incomplete melting.
3. **Layer Thickness:** The thickness of each deposited layer impacts the surface roughness, resolution, and build time. Thinner layers result in finer features but may prolong the overall fabrication process.
4. **Laser Spot Size:** The diameter of the laser beam spot influences the resolution and accuracy of the fabricated parts. Smaller spot sizes enable higher detail but may require longer processing times.
5. **Scan Strategy:** The path followed by the laser beam during scanning, such as contour, hatch, or island scanning, affects the part's mechanical properties and surface finish. Optimal scan strategies minimize residual stresses and porosity while maximizing build efficiency.
6. **Powder Characteristics:** The size, shape, composition, and flowability of the metal powder significantly impact the SLM process. Uniform powder distribution and proper powder handling are essential for achieving consistent part quality.
7. **Build Environment:** Factors such as chamber temperature, inert gas atmosphere, and humidity control influence thermal management and powder bed stability during fabrication. Controlled environments minimize the risk of oxidation, contamination, and warping.

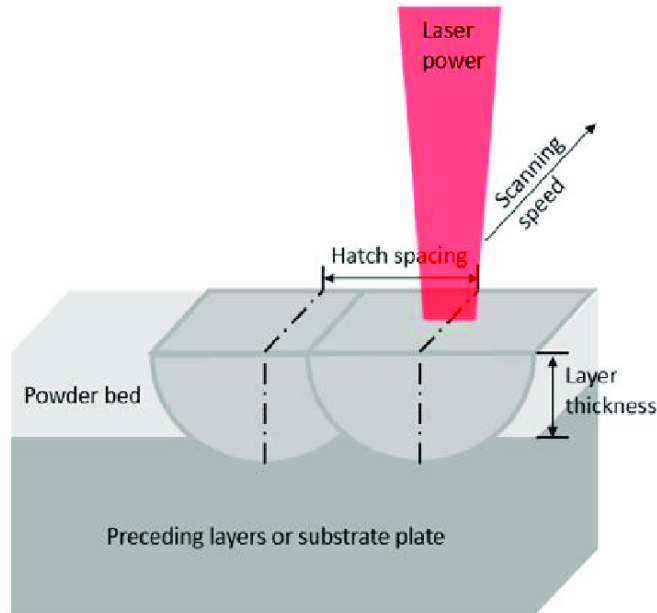


Figure 1. 6: Selective Laser Melting Parameters [22]

Advantages:

compared to conventional production techniques, selective laser melting has the following benefits:

1. **Complex Geometry:** SLM makes it feasible to produce complex geometries that are difficult or impossible to create with traditional machining processes, such as internal channels, lattices, and lightweight structures.
2. **Design Flexibility:** Using SLM, designers may more easily optimize part designs for certain functional needs including part consolidation, weight reduction, and thermal management. Innovation and optimization in product development are made possible by this flexibility.
3. **Material Flexibility:** SLM offers a large selection of metal alloys, such as superalloys based on nickel, titanium, aluminum, and stainless steel. Because of its adaptability, it may be used in a wide range of sectors, from medical implants to aircraft components [19].

4. **Reduced Waste:** Compared to subtractive manufacturing techniques like milling or turning, SLM produces less material waste since it is an additive process. This sustainable advantage lessens the impact on the environment and material prices.
5. **Shorter Lead Times:** SLM enables rapid prototyping and on-demand manufacturing, which reduces lead times and expedites the time it takes for new goods to reach the market. Manufacturing cycle times are shortened, and processes are streamlined when complicated parts may be produced in a single step.
6. **Customization and Personalization:** SLM makes it easier to produce components that are specifically suited to the demands of each particular client or set of application specifications. This skill is especially useful in dentistry and medical applications, where there is a need for prosthesis and implants customized for individual patients.[20].

Disadvantages:

Despite its numerous advantages, Selective Laser Melting has some limitations and challenges:

1. **High Equipment Cost:** SLM machines need complex capital inputs, making them unaffordable for startups and small and medium-sized businesses (SMEs). Adoption may face major obstacles from the initial purchase price to ongoing maintenance and operating costs.
2. **Material Restrictions:** Despite the large variety of metal powders that SLM offers, some materials could be difficult to treat because of their high reactivity, reflectivity, or cracking vulnerability. Depending on the alloy and processing circumstances, material attributes including porosity, surface roughness, and mechanical strength may also change.
3. **Surface Finish and Post-Processing:** Due to the frequent rough surface finishes and residual stress patterns of SLM-produced parts, further post-processing procedures including machining, polishing, and heat treatment are required. These supplementary processes lengthen and complicate the production process.
4. **Dimensional Accuracy and Repeatability:** In SLM, issues including thermal distortion, build orientation, and powder bed compaction can make it difficult to achieve tight

tolerances and consistent product quality. Part-to-part variability and dimensional errors can be caused by changes in material qualities and process conditions.

5. **Support Structures:** To avoid distortion and guarantee construct stability during fabrication, complex geometry and overhanging elements might be required for support structures. Post-processing labor- and time-intensive removal of these support structures can have an impact on efficiency and cost-effectiveness.
6. **Material Properties and Microstructure:** SLM's accelerated rates of solidification can result in irregular microstructures, anisotropic mechanical characteristics, and a vulnerability to flaws including porosity, cracking, and lack of fusion. To achieve the desired material qualities and performance characteristics, process parameters and heat treatment regimens must be optimized. [21].

1.1.4.3 3D Printing of Ti6Al4V Using Selective Laser Melting Techniques

Titanium alloys are highly sought-after materials in various industries due to their exceptional combination of strength, corrosion resistance, and biocompatibility. Among these alloys, Ti6Al4V (Titanium-6 Aluminum-4 Vanadium) is particularly popular for its favorable mechanical properties, making it an ideal candidate for aerospace, medical, and automotive applications. With the advent of additive manufacturing technologies, such as Selective Laser Melting (SLM), the production of complex Ti6Al4V components with intricate geometries and superior mechanical performance has become feasible [22].

In the case of Ti6Al4V, titanium and aluminum powders are mixed with a precise ratio of vanadium to achieve the desired alloy composition. The powder bed is spread uniformly onto the build platform, and a high-energy laser beam is directed onto specific areas based on the CAD model. The intense heat generated by the laser rapidly melts the metal powder, which solidifies upon cooling, effectively bonding to the previous layer. This process is repeated layer by layer until the final part is formed[23]. Below are some of lightweight additively manufactured by Selective laser melting from titanium alloy.



Figure 1. 7: 3D printed titanium parts: Hip joints, fan blade, rocket tip, titanium lattice component, titanium bracket, surgical spinal implant[24]

1.1.4.4 Advantages of 3D Printing Ti6Al4V with SLM:

Complex Geometries: SLM enables the fabrication of Ti6Al4V components with intricate geometries that would be challenging or impossible to produce using traditional manufacturing methods. This capability allows for the optimization of part designs to improve functionality and performance.

Material Efficiency: Additive manufacturing processes like SLM generate minimal material waste compared to subtractive methods, such as machining. This efficiency not only reduces material costs but also contributes to sustainability efforts by minimizing environmental impact.

Customization: 3D printing Ti6Al4V with SLM offers the flexibility to produce customized parts tailored to specific applications or individual requirements. This customization capability is particularly valuable in the medical field for producing patient-specific implants and prosthetics.

Shorter Lead Times: SLM allows for rapid prototyping and on-demand production of Ti6Al4V components, leading to shorter lead times and faster time-to-market for new products. The ability to iterate designs quickly facilitates the development process and accelerates innovation.

Enhanced Mechanical Properties: Parts manufactured using SLM exhibit superior mechanical properties compared to conventionally produced components. The fine microstructure and near-net shape fabrication result in enhanced strength, fatigue resistance, and overall performance of Ti6Al4V parts.

Reduced Assembly Requirements: With SLM, complex assemblies can be consolidated into single components, reducing the need for joining techniques like welding or brazing. This consolidation not only simplifies the manufacturing process but also eliminates potential weak points and reduces assembly time and costs[25].

1.1.4.5 Challenges and Considerations:

Cost of Equipment: SLM machines are sophisticated and expensive, requiring significant capital investment. Additionally, operating and maintenance costs can be substantial, particularly for ensuring process reliability and quality control.

Material Properties and Processing Parameters: Achieving optimal material properties and part quality with Ti6Al4V requires careful control of processing parameters, including laser power, scanning speed, and powder characteristics. Variations in these parameters can lead to defects such as porosity, residual stresses, and dimensional inaccuracies.

Surface Finish and Post-Processing: Parts fabricated with SLM typically exhibit rough surface finishes and may require post-processing steps such as machining, polishing, or heat treatment to achieve the desired surface quality and dimensional accuracy. These additional steps can add time, cost, and complexity to the manufacturing process.

Support Structures: Complex geometry and overhanging features may require the use of support structures to prevent distortion and ensure build stability during fabrication. However, removing these support structures post-processing can be labor-intensive and may leave behind surface imperfections.

Material Degradation: The intense heat generated during SLM can lead to material degradation, such as grain growth and phase transformations, which may affect the mechanical properties and

microstructure of Ti6Al4V parts. Proper heat treatment and process optimization are essential to mitigate these effects and ensure consistent part quality[26].

1.1.5 Applications of 3D Printed Ti6Al4V Components:

Aerospace: Ti6Al4V components manufactured with SLM are utilized in aerospace applications, including structural components, engine parts, and heat exchangers, due to their lightweight, high strength-to-weight ratio, and corrosion resistance[27].

Medical: In the medical field, 3D printed Ti6Al4V implants, such as orthopedic implants and dental prosthetics, offer patient-specific solutions with excellent biocompatibility and osseointegration properties, improving patient outcomes and recovery times.

Automotive: Ti6Al4V parts produced using SLM find applications in automotive engineering for lightweighting initiatives, performance enhancements, and functional prototypes, contributing to fuel efficiency, vehicle performance, and design innovation.

Tooling and Jigs: Additively manufactured Ti6Al4V tooling and jigs are used in various industries for manufacturing processes such as forming, casting, and machining, offering durability, precision, and cost-effectiveness compared to conventional tooling methods.

Defense and Aerospace: Ti6Al4V components play a critical role in defense and aerospace applications due to their high strength, fatigue resistance, and ability to withstand harsh environments. Additive manufacturing enables the production of complex, lightweight parts with reduced lead times and cost [28].

In conclusion, 3D printing of Ti6Al4V using Selective Laser Melting (SLM) techniques offers numerous advantages, including the ability to produce complex geometries, customization, and enhanced mechanical properties. Despite challenges such as equipment costs, material considerations, and post-processing requirements, the versatility and performance of Ti6Al4V parts manufactured with SLM make them highly desirable for a wide range of applications across industries. As technology continues to advance and process optimization efforts progress, the adoption of additive manufacturing for Ti6Al4V components is expected to increase, driving innovation, and unlocking new possibilities in engineering and design[29].

1.1.6 Aerospace Industry and AM:

AM is gaining traction as a cost-effective fabrication process for the aerospace industry's supply chain and maintenance operations. The aerospace industry is one of the top areas driving the AM market over the past decade. In the AM sector, the aerospace industry now contributes 18.2 per cent of revenues. With a 1.6 per cent annual rise in 2016, the aerospace industry is also the fastest growing, the motor vehicles at second with a 1.0 per cent increase. AM revenues are estimated to reach \$2.7 billion in 2016 (up 12.9% from 2015) and to top \$100 billion over the next two decades, particularly in the aerospace industry. Metal and nonmetallic (primarily polymer) components are commonly associated with critical and noncritical aircraft parts, respectively, in the aerospace market for AM parts [30].

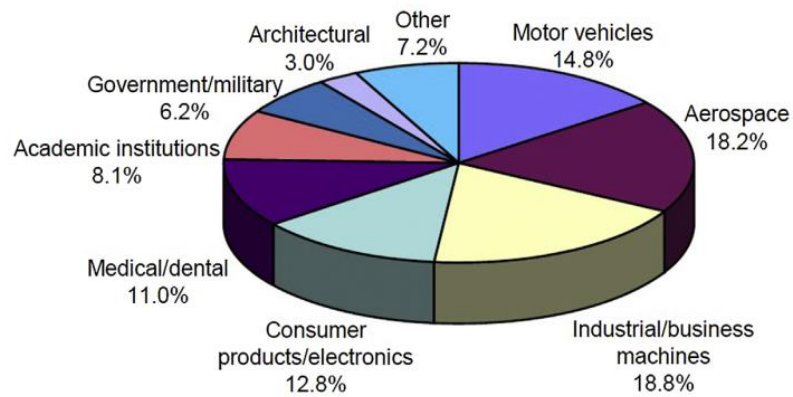


Figure 1. 8: AM Additive Manufacturing market share [27]

1.1.6.1 Aircraft structure

Fixed-wing aircraft are the most prevalent type of aircraft. The wings of this sort of flying vehicle, as the name implies, are connected through joints to the fuselage, and are fit tight so they can't move independently. The wings are designed in a way to create lift force required for flight. The following schematic shows the basic components of a fixed-wing aircraft [31].

In unaccelerated straight and level flight, four forces act on an aircraft. Thrust, lift, weight, and drag are examples of these forces.

Thrust is the forward force generated by the engine/propeller. It opposes or overcomes the drag force. It is believed to act parallel to the longitudinal axis in general. Drag is a backward, slowing force created by the wing, fuselage, and other projecting structures disrupting airflow. Drag acts in the opposite direction of push, parallel to the relative wind.

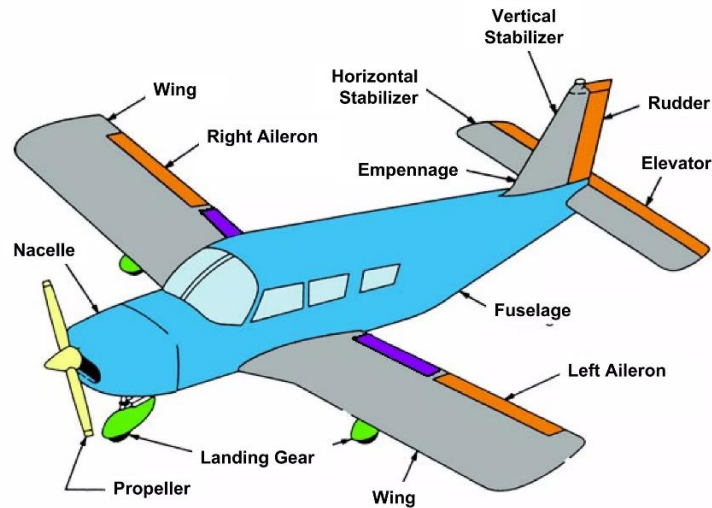


Figure 1. 9: Components of fixed-wing aircraft[32]

Drag is a backward, retarding force created by the wing, fuselage, and other projecting items disrupting airflow. Drag resists push and acts in the opposite direction of the relative wind.

The aggregate weight of the aeroplane, the crew, the fuel, and the cargo or baggage is the weight. Because of the force of gravity, weight pulls the plane downward. It works vertically downward through the aeroplane's centre of gravity, opposing lift (CG)

1.1.6.2 Vertical Control Surface:

The vertical stabilizer, often referred to as the tail fin, is a fixed vertical surface located at the rear of an aircraft. It is very crucial component of an aircraft's empennage (tail section) and plays a vital role in maintaining the aircraft's stability and control during flight.

1.Function and Purpose:

The primary purpose of the vertical stabilizer is to provide control, stability, and trim in the yaw axis (also known as directional stability). It compensates for moments generated by asymmetry in thrust or drag, allowing the aircraft to maintain a straight course during flight. Additionally, it enables controlled yaw maneuvers, such as initiating side slip during crosswind landings.

2. Design and Structure:

The design and structure of the vertical stabilizer are aerodynamically optimized to provide maximum stability with minimum drag. It typically has a streamlined shape to reduce drag and is often attached to the rear portion of the fuselage or tail section of the aircraft.

3. Materials:

Vertical stabilizers are usually made of lightweight, high-strength materials such as aluminium alloys, titanium, or composite materials. These materials are chosen for their strength, durability, and weight-saving properties.

4.Position and Effectiveness:

The effectiveness of the vertical tail depends on its efficiency and the vertical tail volume coefficient. Shorter aircraft typically feature larger vertical tails to enhance stability. The vertical tail's position away from the centre of gravity influences its effectiveness [33].

In aerospace, especially aviation, reducing weight is directly related to improving fuel efficiency. For a specific range profile, a lighter aircraft or spacecraft requires less fuel to be carried. Weight reduction is a conceptual challenge for engineers and designers, stimulating new developments in manufacturing processes, materials science, and overall vehicle design[27]. Weight reduction allows for a higher payload capacity. This is crucial for space exploration since carrying more people, cargo, or scientific equipment may be constrained by the ship's weight. The weight of the spacecraft may be kept to a minimum, creating more room for valuable payloads. Lighter aircraft may travel longer or survive in flight for longer, which is vital for various aerospace applications[34]. Due to superior thrust-to-weight ratios, more lightweight aircraft can fly faster

and at higher altitudes. During flight, a lighter aircraft experiences less stress on its structural parts, which might result in longer operating lifespans and fewer frequent maintenance requirements[35]. Lighter aerospace vehicles have less overall environmental effects since they use less fuel and emit fewer pollutants. For aerospace manufacturing and research companies, achieving weight reduction can lead to a competitive advantage by offering more efficient and capable aerospace solutions. AM technology is best suited for aerospace applications because of the growing need for intricate and lightweight metal components, particularly from the aerospace industry[36].

Michael Süß used the topological optimization method to redesign the gearbox of helicopter satisfying all the loading, boundary, and strength constraints. These redesigns achieved significant weight reduction up to 40% without major impact on their mechanical behavior. Components were subsequently manufactured using Electron beam melting (EBM) technology, demonstrating the feasibility of combining optimization and AM concepts for future aerospace structures[37]. Lopez-Castro did mass optimization of 56% in an aeronautical bracket manufactured from AISI 15-5PH stainless steel instead of Titanium alloy by Direct Laser melting Sintering. It offers the same mechanical properties with lower cost with a density of 1.7 times Titanium alloy [38]. David J. Munk designed landing gear for a lightweight aircraft. It was concluded that using topology optimization, 40% mass reduction could be obtained compared to standard engineering practice while still complying with the Federal Aviation Regulation [39]. Akin Dagkolu did 45% mass reduction achieved through optimization while ensuring compliance with stringent mechanical requirements. To address thermal distortions during manufacturing, simulations were conducted. The optimized part was then successfully manufactured using laser powder bed fusion (L-PBF), supplemented by secondary operations [40]. Yun-feng Liu designed customized fixation plate with novel structure by topology optimization for mandibular angle fracture based on finite element analysis. The customized fixation plate demonstrated reduced stress, strain, and displacement additively manufactured by Selective laser melting technique[41]. Kangjie Cheng successfully modeled and optimized mandibular bone of a beagle dog including a customized external shape, supporting structures and micro-pores leading to a remarkable weight reduction of 37.2% additively manufactured by selective laser melting technique and the implant compliance was significantly reduced by 53.3 %[42]. RONG LIU designs orthopedic scaffolds and fabricates using selective laser melting technique. The resulting structures resemble natural bone and exhibit

satisfying mechanical performance and porosity similar to cancellous bone [43]. Oliver Bittredge designed and optimized a cellular-based lattice-structured implant for controlling the stiffness of humeral implant stems in shoulder applications. Lattice-optimization tool was Employed to create diverse cellular designs within the original shoulder implant framework and selective laser melting technique was used to create Ti-6Al-4V test samples. Implant Weight Reduction was Up to 44% compared to fully solid implants [44].

Although SLMed titanium alloys have certain distinct characteristics, they still exhibit common 3D printing problems including porosity, residual stress, and microstructure defects. These layer-based AM techniques are prone to induce residual stresses because of their inherent larger temperature gradients. The residual stresses increase with increasing layer thickness and maximum value always found at the free surface of final layer. Vastola calculated the effect of pre-heating temperature of the bed fusion and found that increment of 50C reduces stress by 20%. Another way used for stress relieving is post-processing heat treatment[45]. Li et al perform tensile testing on Additive manufactured parts at both high and low strain rates with increased temperature. Ductile dimples were seen in high-strain-rate fractures, whereas the tensile fractures showed composite fracturing morphologies at low strain rates, containing both quasi-cleavages and dimples. The tensile strength dropped by 60% because of an increase of temperature from 273k to 1173k due to reduction in dislocation density[46]. Lueders investigated correlation of microstructure-defect property for SLM processed Ti6Al4V alloy under cyclic loading. It is determined that micro pores mainly affect fatigue strength while residual stresses have a strong effect on fatigue crack propagation[47]. Karolina tested mechanical properties and macrostructure before and after failure of Titanium alloy manufactured by Direct metal laser sintering and drawn bar by turning process. The strength of sample made by DMLS additive technology is greater than sample made of drawn rod while value of Young`s Modulus for both the methods were same[48]. X.P Ren did a comprehensive study on comparison of mechanical properties and microstructure of Ti6Al4v alloy manufactured by SLM, EBM and Mill annealing. Many studies have presented the relationship between the microstructure properties of Ti alloy and the produced process i.e. SLM, EBM and mill annealing[49].

1.2 Problem statement

The optimization of aero vehicle control surfaces is essential to reduce material waste, fuel consumption, and production costs. Currently, these surfaces are fabricated from solid blocks of Titanium alloy (Ti6Al4V), resulting in significant material wastage. Hence, there is a critical need to minimize the mass of control surfaces while ensuring efficient performance, thereby saving both material and production resources.

1.3 Objectives:

- The Objectives of this Research are:
- Design and Manufacturing of an aero vehicle control surface by Selective Laser Melting Technique (SLM) to obtain low mass as compared to the conventional manufacturing for the same strength and application.
- Material characterization of the samples produced by SLM technique and their comparison with the traditional manufacturing methods.
- Comparison of the properties Obtained from Testing assigned to new design and standard properties assigned to solid control surface design Through Finite Element Analysis (FEA).

1.4 Scope:

In current study

- Aero vehicle control surface will be designed and additively Manufactured using SLM technique with reduced mass as compared to conventional manufacturing techniques.
- Mechanical properties i.e. tensile strength, fracture toughness and hardness of SLM printed Ti6AL4V samples will be measured and compared with the conventional manufacturing technique.

- Thermal properties, i.e. thermal conductivity, coefficient of thermal expansion and specific heat of SLM printed Ti6AL4V samples will be measured and compared with the conventional manufacturing technique.
- Validation of control surface by FEA will be performed and compared with the standard properties of Ti6Al4V alloy.

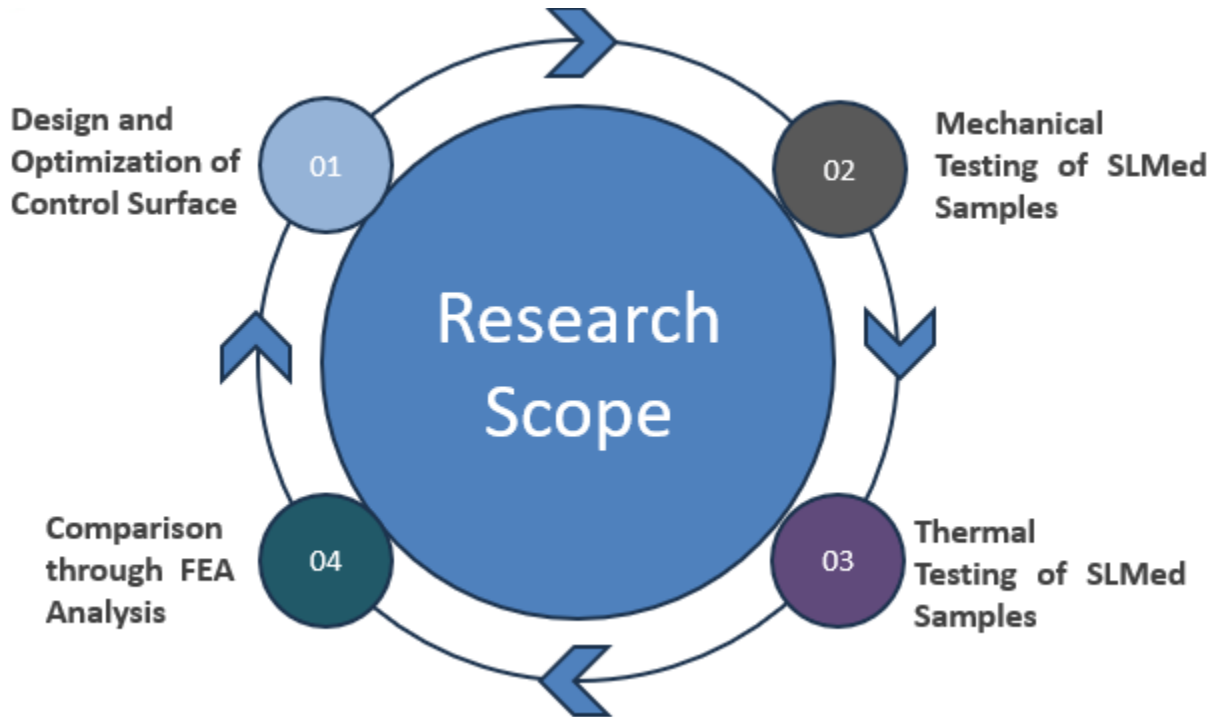


Figure 1. 10: Visualizing the Research Scope and Sequential Stages

CHAPTER 2: MATERIALS AND METHOD

This chapter focuses on design and optimization of control surface, characterization of Ti6Al4V alloy, numerical analyses of control surfaces with both standard and tested properties and their comparison, manufacturing of control surface through Selective laser melting technique. The raw material used was 99% pure Ti6Al4V alloy powder and samples were printed using a Farsoon machine by selective laser melting technique. Experimental procedures and testing are reported along with all fabrication and characterization techniques. The methodology followed for the overall study is shown in figure 2.1.

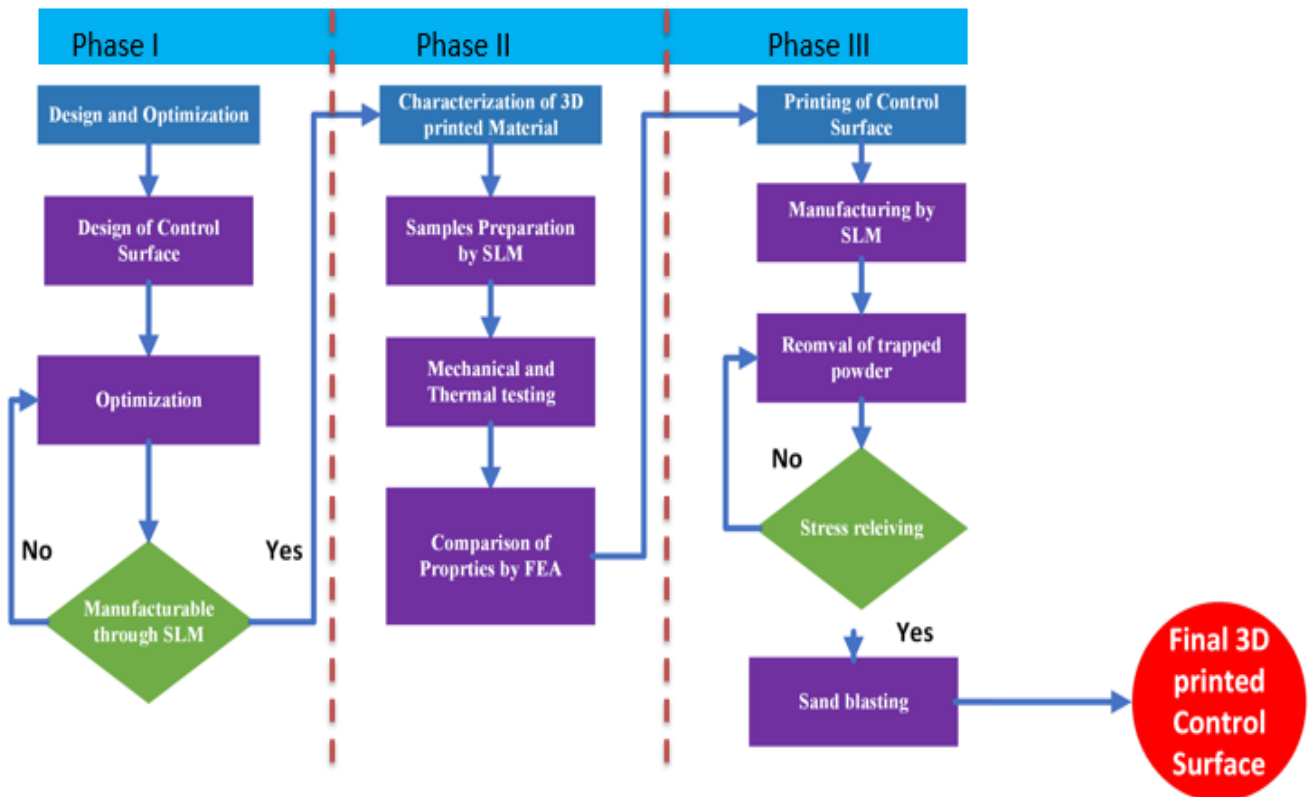


Figure 2. 1: Research Methodology Flowchart

2.1 Design of control surface

For design optimization of aero vehicle control surface various iterations were performed to minimize the mass for the same structural and thermal loading conditions. Initially the fin was designed with pockets at leading and trailing sides to align CG of control surface with shaft. The mass minimization was less. The sketch is shown in figure 2.2.

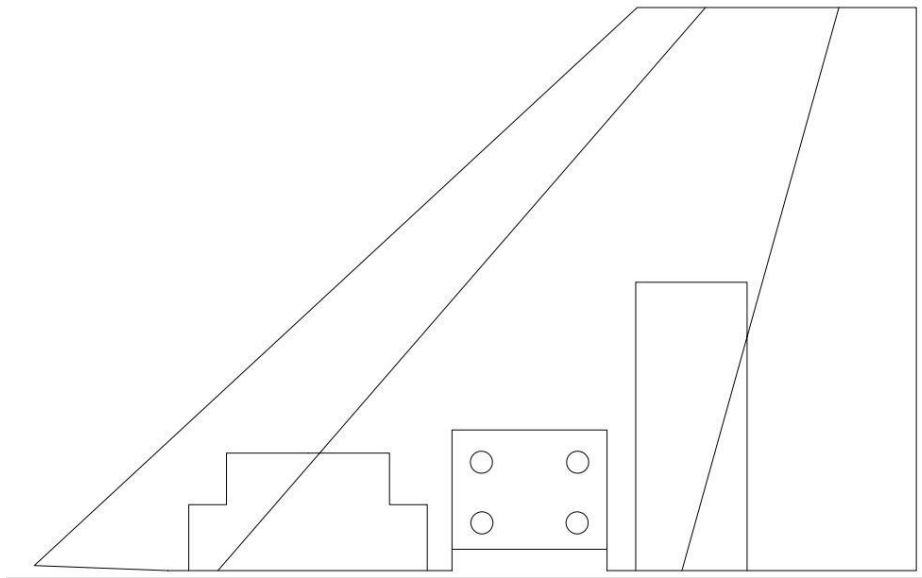


Figure 2. 2: Initial Solid Design With leading and trailing sides

In the second iteration a honeycomb structure was used to reduce mass and attain structural stability, but the idea was dropped due to manufacturing constraint of selective laser melting technique as the metal powder will be trapped in honeycomb cells. The sketch is shown in figure 2.3.

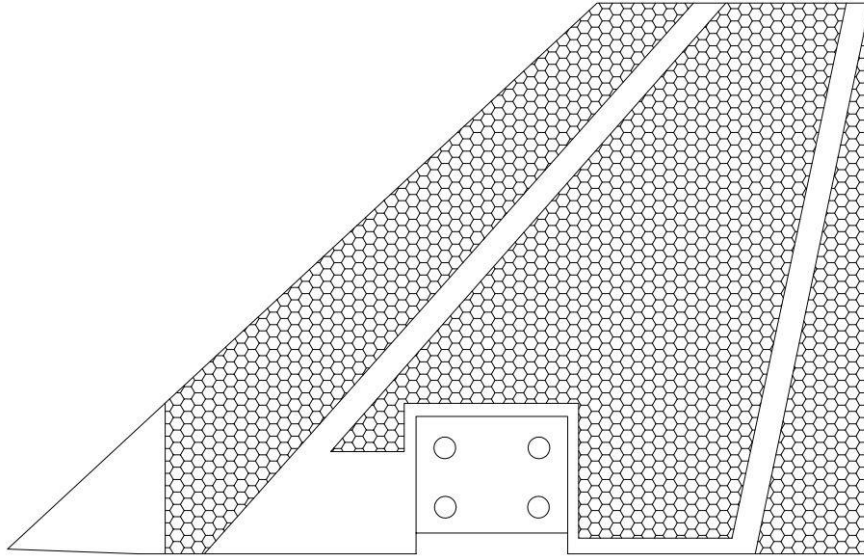


Figure 2. 3: Honeycomb structure

In further iterations, ribbed structures were used to provide extra strength in bending, and pockets were introduced along with the slots at each pocket exit location for removal of powdered metal from inside the body. In successive iterations the outer skin of the control surface and ribs were reduced to improve mass saving. The mass of the final machined control surface was 53% less than extracted from solid block of Ti6Al4V. The sketch is shown in figure 2.4.

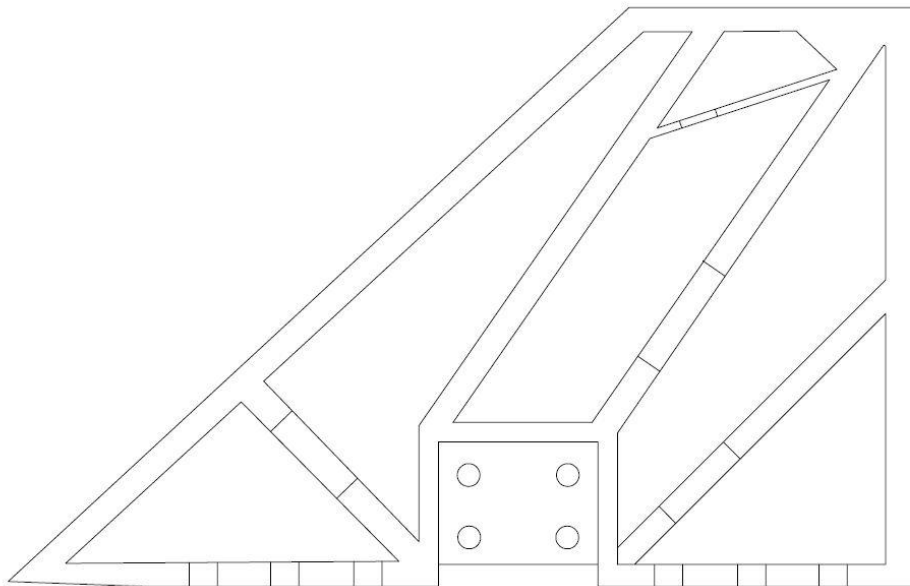


Figure 2. 4: Ribbed Structure

2.2 Fabrication of samples

Farsoon FS421M Machine was used to fabricate the Ti6Al4V specimens through SLM as shown in figure 2.5. The FS421M Machine combines advanced technology, large build volume, and precise control to fabricate high-quality metal samples. Specifications of the machine are given in table2.1.



Figure 2. 5: Farsoon FS421M machine for printing of test specimens through SLM[50]

Table 2.1: Specifications of FARSOON Machine

S. No.	Material	Titanium alloy (Ti6Al4V)
1	Bed size	420mmx420mm
2	Powder layer thickness	40 microns
3	Layer deposition interval	10 sec
4	Surface finish	8.5 microns
5	Machine accuracy	0.1 mm
6	Max. height of part without supports	40 mm
7	Min. wall thickness	0.3 mm

Samples were modelled in SolidWorks and exported in STL format and loaded onto the PC. The samples were automatically sliced into layers using machine's software and printed according to the ASTM standards for different testing selecting the parameters given in table2. Maximum laser power of 280watts was used with scanning speed of 1200mm/s.

Table 2.2: Printing parameters for Printing Samples

S. No.	Parameters	Value
1	Laser Power	280 watts
2	Laser spot	100 μm
3	Scanning speed	1200 mm\s
4	Hatch distance	80 μm
5	Layer thickness	40 μm

2.3 Tensile testing:

Samples were fabricated using Selective Laser Melting (SLM) technique for the purpose of conducting tensile tests across various temperature conditions. A total of eight samples were manufactured and subsequently evaluated using a Universal Testing Machine (UTM) with a strain rate of 2mm/min at room temperature and five samples are printed for testing at elevated temperatures as shown in figure 2.6 & 2.7 respectively.



Figure 2. 6: samples for testing at room temperature



Figure 2. 7: samples for testing at elevated temperatures



Figure 2. 8: UTM with furnace for elevated temperature testing[51]

Testing procedures were conducted in accordance with ASTM E8M-4 standard at room temperature and GB 228 standard at elevated temperatures of 200°C, 400°C, and 600°C. The dimensions for samples according to ASTM E8M-4 are shown in figure 2.9.

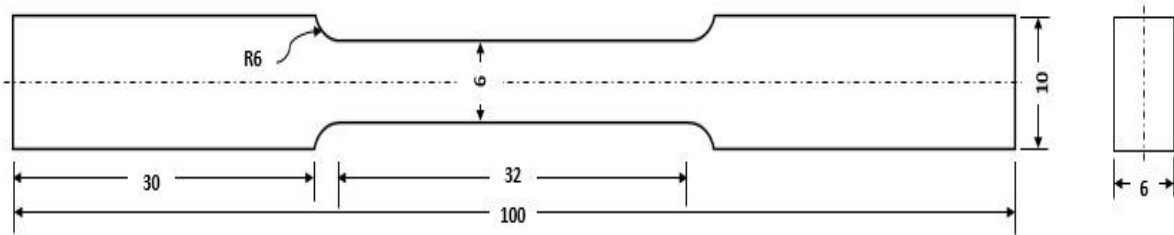


Figure 2. 9: Dimensions of tensile testing sample at Room Temperature

To achieve the desired testing temperatures, a controlled heating system was employed. The samples were subjected to elevated temperatures using a clamping furnace, ensuring uniform heating throughout the specimens. Once heated, the samples were securely clamped within the UTM and subjected to tensile testing at the respective temperatures: 200°C, 400°C, and 600°C. The yield strength, Tensile strength, young`s Modulus and %age elongation is measured from the stress strain curve obtained. The dimensions of samples according to GB 228 are shown in figure 2.10.

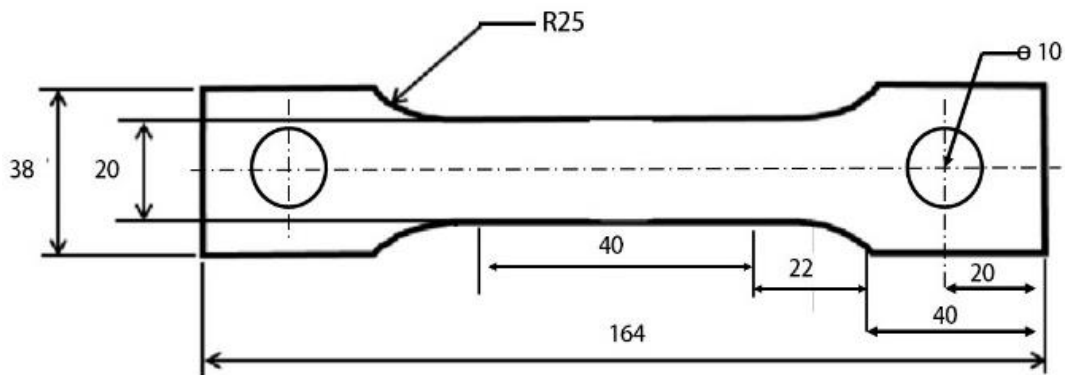


Figure 2. 10: Dimensions of tensile testing sample at elevated temperatures

During testing, parameters including yield strength, tensile strength, Young's Modulus, and percentage elongation were measured to characterize the mechanical properties of the samples under the specified temperature conditions.

$$\text{Normal Stress} = \sigma = \frac{F}{A}$$

$$\text{Normal Strain} = \frac{\Delta L}{L}$$

$$\% \text{age Elongation} = \frac{\Delta L}{L} \times 100$$

$$\text{Young's Modulus} = E = \frac{\text{Normal Stress}}{\text{Normal Strain}}$$

$$E = \frac{F \times L}{A \times \Delta L}$$

where

E is Young's Modulus,

σ is the normal stress,

ϵ is the normal strain,

F is the applied force,

L is the original length, and

A is the cross-sectional area.

2.4 3 Point bending test:

Three-point bend testing was performed on 03 printed samples according to ASTM E 399 to measure fracture toughness at room temperature. A machine that delivers a load at two sites and supports the specimen at a third is usually used to apply a specimen to a bending force in this test[52]. Flexural testing is used to evaluate the mechanical properties of materials, specifically their bending strength and stiffness. The dimensions of the sample are shown in figure 2.11. An initial fatigue crack was created by cyclic loading and crack length was measured. Monotonic load was applied, and load vs crack opening displacement data was recorded. Bending strength,

Flexural Modulus and critical stress intensity factor are measured from the load vs crack opening displacement curve obtained using equations given below.

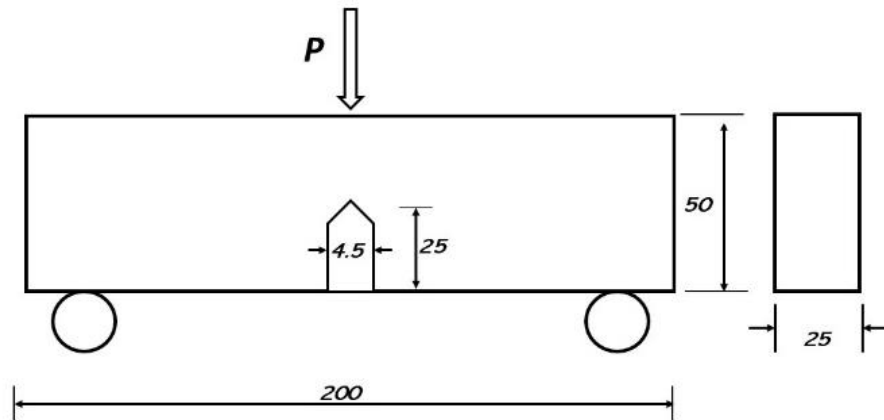


Figure 2. 11: Dimensions of Fracture toughness sample

$$\text{Bending stress} = \sigma_b = \frac{MC}{I}$$

$$\text{Bending strain} = \epsilon_b = \frac{6Dd}{L^2}$$

$$\text{Flexural Modulus} = \frac{\sigma_b}{\epsilon_b}$$

$$\text{Stress intensity factor} = K_{IC} = \frac{F*L}{B*W^2} * f\left(\frac{a}{W}\right)$$

Where

F= Max load applied

L= Span length

b= Sample thickness

w = Sample height

D= Max deflection

B= Sample thickness

f(a/W): Correction factor based on the crack length (a) and specimen width (W)[53]

2.5 Rockwell Hardness Test:

Hardness of 3D printed Ti6Al4V is found according to ASTM E 10 standard on Rockwell hardness tester with Diamond cone indenter. The type C scale is used to measure the hardness as Ti6Al4V is medium harder material according to the formula.

$$HRC = 100 - \frac{\text{change in depth}(mm)}{0.002} [54]$$

An initial load of 98N was applied on specimen of 25x25x4 to set contact between specimen and indenter after that load of 150 kg is applied for short interval and then removed. The hardness value is measured from the permanent indentation in the sample[55].



Figure 2. 12: Rockwell hardness tester machine[56]

2.6 Thermal Conductivity test by GHFM:

Thermal conductivity of 3D printed sample is measured according to ASTM E 1530 standard on Guarded heat flow meter. 4 samples of 7mm thickness and 50 mm dia are printed and tested at different temperatures, shown in figure below. The sample is placed in GHFM, and upper, lower temperatures are set to apply temperature gradient. Thermal conductivity is calculated according to Fourier formula given below at RT, 100C, 200C and 300C steady state through thickness temperature.

During the experimental setup, a load, or force, is applied from the top, causing compression of the sample. The upper plate, denoted as “Tu,” directly bears the load. Positioned between the upper and lower plates is the sample itself, labeled “Tl.” Temperature measurements are taken at both the upper and lower surfaces of the sample to monitor thermal changes.



Figure 2. 13: samples for thermal conductivity test

To assess heat flow through the sample, a heat flow meter is situated beneath the lower plate. This device quantifies the heat passing through the sample, attributable to the temperature gradient established within it. Furthermore, to maintain a stable temperature gradient and ensure precise

measurements, a heat sink is implemented at the bottom of the system. This component efficiently dissipates excess heat away from the setup.

To safeguard against external temperature fluctuations, a guard furnace is positioned on the right side. This furnace consistently sustains a uniform temperature surrounding the entire experimental arrangement. By doing so, it mitigates the risk of external influences skewing the accuracy of the measurements, thus enhancing the reliability of the experimental results.



Figure 2. 14: Guarded heat flow meter[57]

$$R_{sam} = \frac{t}{\lambda} = f_{con} \frac{T_u - T_l}{Q} - R_{con}$$

Where

R_{con} = thermal resistance of interface

Q = heat flow from transducer output

T_l = surface temperature of lower plate

T_u = surface temperature of upper plate

f_{con} = heat flow transducer calibration factor

R_s = sample thermal resistance [58]

2.7 Thermal Coefficient of Expansion test by Dilatometer (DIL-402C):

Thermal coefficient of expansion of 3D printed samples of length 25 mm and dia 6mm are tested at room temperature, 100, 200, 300, 400, 500 & 600 according to ASTM E228 on Dilatometer (DIL-402C).



Figure 2. 15: Dilatometer (DIL-402C)[59]

The temperature was set to range between 10°C and 700°C .sample was placed and aligned with the vitreous silica pushrod in the dilatometer to minimize any angular miss alignment. After achieving thermal equilibrium, temperature gradually increased, and expansion of samples are monitored with the change in temperature.

Change in length vs temperature was recorded and CTE was calculated using the following equation:

$$\alpha = \Delta L / L_0 \cdot \Delta T$$

Where:

ΔL : Change in length of the sample

L_0 : Initial length of the sample at the reference temperature

ΔT : Temperature difference ($T_2 - T_1$)[60]

In this testing setup, a linear motor is positioned at the top to apply a precisely controlled force or displacement to the system. Directly below the linear motor, a displacement sensor is installed to monitor any changes in length or displacement of the sample. The displacement sensor comprises two parallel lines and serves to measure the extent of deformation experienced by the sample under the applied force.

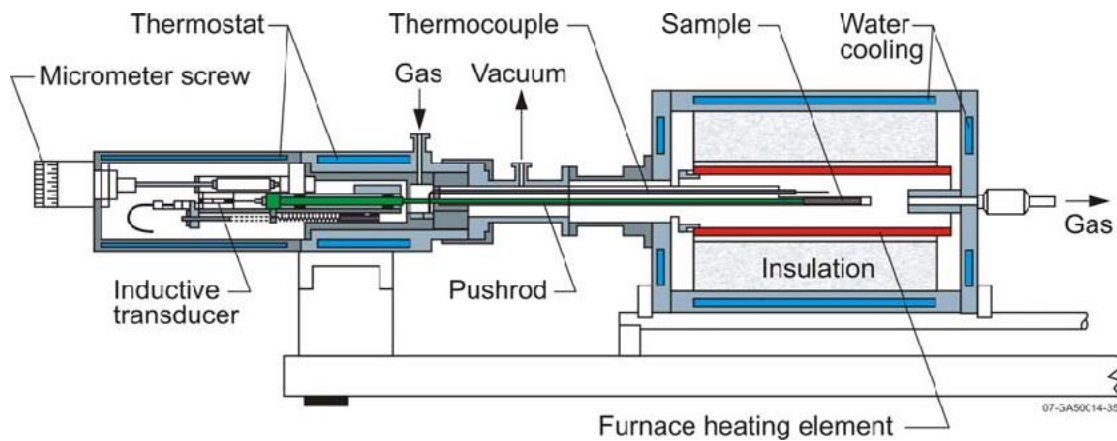


Figure 2. 16: Push rod Dilatometer[61]

To transmit the force from the linear motor to the sample, a push rod extends downward from the displacement sensor. This push rod acts as a conduit, ensuring the transfer of force to the sample in a consistent and controlled manner. At the bottom of the push rod lies the sample being tested, represented by a green rectangle. The material of this sample is subject to expansion or contraction in response to changes in temperature.

Surrounding the sample, outlined by red rectangles on either side, are furnaces. These furnaces are responsible for providing regulated heating to the sample throughout the duration of the test. By maintaining a constant and controlled temperature environment, the furnaces facilitate accurate evaluation of how the sample material behaves under varying thermal conditions.

2.8 Specific Heat capacity test by differential scanning calorimeter:

Specific heat capacity of Ti6Al4V powder is measured according to ASTM E 1269 at room temperature, 100, 200, 300, 400, 500 & 600C° on differential scanning calorimeter. According to the sapphire method, blank curve was obtained in first step with both crucibles empty. In the second step specific heat capacity of reference sample is obtained and third step reference sample was replaced by Ti6Al4V powder to measure specific heat capacity at Room temperature and up to 600C°.



Figure 2. 17: sample for DSC test



Figure 2. 18: Differential Scanning Calorimeter[62]

$$C_{p,p} = \frac{\theta_p - \theta_0}{\theta_{sap} - \theta_0} \cdot \frac{m_{sap}}{m_p} \cdot C_{p,sap}$$

$C_{p,p}$: specific heat capacity of the sample

$C_{p,sap}$: specific heat capacity of the sapphire reference

θ_p : heat flow of the sample

θ_0 : heat flow of the blank curve

θ_{sap} : heat flow of the sapphire reference

m_{sap} : mass of the sapphire reference

m_p : mass of the sample[63]

2.9 Numerical Simulation Setup:

ANSYS Workbench 2020R2 is used to perform structural Analysis, the Static Structural module was employed to evaluate both the initial and final optimized designs. Material properties were assigned to both designs based on the engineering data, and the designs were imported into ANSYS Mechanical for the analysis. The Hex Dominant method is used for meshing with mesh size of 5mm for structure assembly and 1mm size for bolts. Connections are made as per actual attachment of the assemblies. Bolted assemblies have standard contacts while remaining have bonded contacts to transfer load as per real scenario in the loading condition.

A cylindrical support was applied to the lower mount of the structure to simulate the boundary conditions. Additionally, loads were applied to the structure in both axial and normal directions to assess its structural performance under operating conditions shown in figure 2.19.

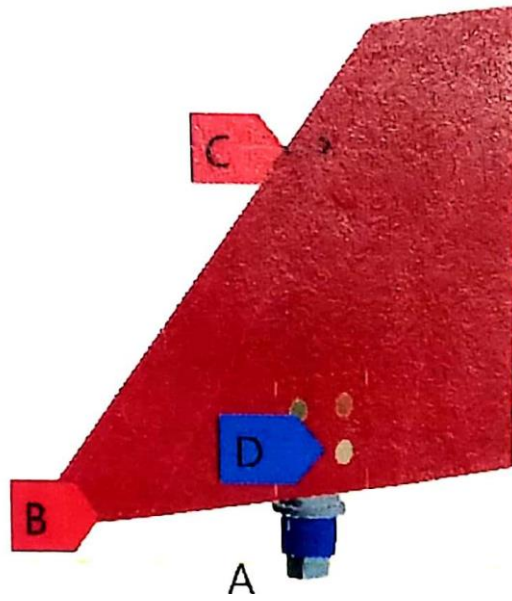


Figure 2. 19: Boundary Conditions

For the initial design, standard properties of Ti6Al4V were assigned to simulate its material characteristics. In contrast, the final optimized design was assigned the tested properties of the material. Structural analysis was then conducted on both designs using the Static Structural module in ANSYS Workbench 2020R2 to perform a comparative analysis of their performance and behavior under the specified loading conditions.

CHAPTER 3: RESULTS

3.1 Optimized Control Surface Design:

In the process of optimizing the design of an aero vehicle control surface, several iterations were undertaken to minimize mass while maintaining structural and thermal integrity. The initial fin design incorporated pockets at both the leading and trailing edges to align the control surface's center of gravity (CG) with the shaft. However, the mass reduction achieved was insufficient. In the second iteration, a honeycomb structure was employed to reduce mass and enhance structural stability. Unfortunately, this idea was abandoned due to manufacturing constraints associated with selective laser melting. The risk of metal powder becoming trapped within the honeycomb cells posed challenges. Subsequent iterations introduced ribbed structures. These ribs provided additional strength, particularly in bending scenarios. To facilitate the removal of powdered metal from within the body, pockets were strategically placed along with slots at each pocket exit location as shown in figure. As the optimization process continued, the outer skin of the control surface and the ribs underwent further reduction. The mass of the final machined control surface was 53% less than extracted from solid block of Ti6Al4V. After rigorous exploration, the ribbed structure emerged as the final optimized design. It not only minimized mass but also ensured the necessary strength and functionality.

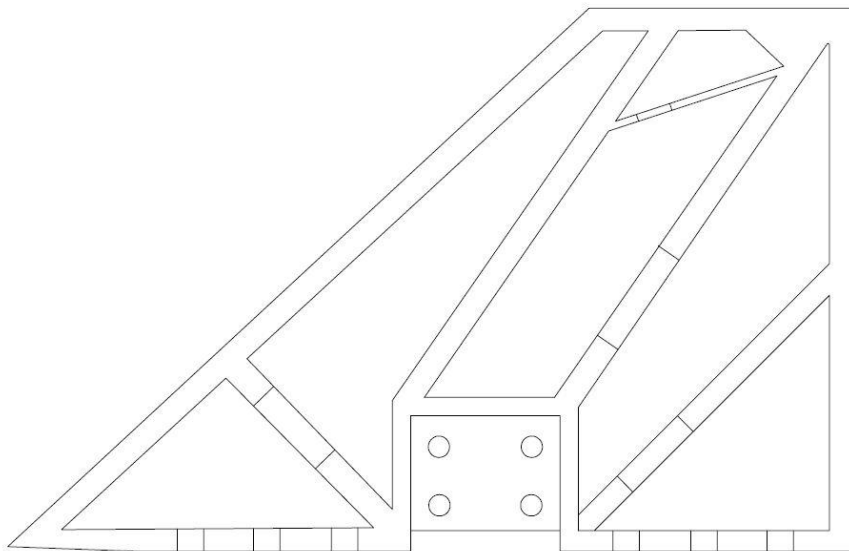


Figure 3. 1: Final Optimized ribbed structure Control Surface

3.2 Fabricated samples by FARSOON machine:

The FS421M Machine, equipped with advanced technology, a spacious build volume, and precise control, was employed to fabricate high-quality metal samples. Utilizing titanium alloy (Ti6Al4V) as the material, the machine featured a bed size of 420mm x 420mm. The powder layer thickness was set at 40 microns, and layer deposition occurred at intervals of 10 seconds. With an impressive accuracy of 0.1 mm and achieving a surface finish of 8.5 microns, the machine showcased its capability. Notably, the maximum height of a part without supports was 40 mm, and the minimum wall thickness allowed was 0.3 mm.

The fabrication process began with the design phase in SolidWorks, where models were meticulously crafted and exported in STL format. These STL files were then loaded onto the PC connected to the machine. Utilizing the machine's software, the samples were automatically sliced into layers in compliance with ASTM standards for various testing scenarios. The fabrication involved a maximum laser power of 280 watts and a rapid scanning speed of 1200 mm/s. Some of the samples printed by FARSOON Machine are given in figure 3.2.



Figure 3. 2: 3D Printed sample by FARSOON Machine

3.3 Tensile testing Results:

Tensile testing was conducted on the material specimens both at room temperature (RT) and at elevated temperatures of 200°C, 400°C, and 600°C. At RT, the material behaved typically for metals, showing a sharp increase in stress until it reached its yield point at 938 MPa. After this, the material started deforming plastically, and the stress-strain curve flattened, indicating strain hardening. It finally fractured at an elongation of 9.2%, with an ultimate tensile strength (UTS) of 952 MPa as shown in figure 3.3.

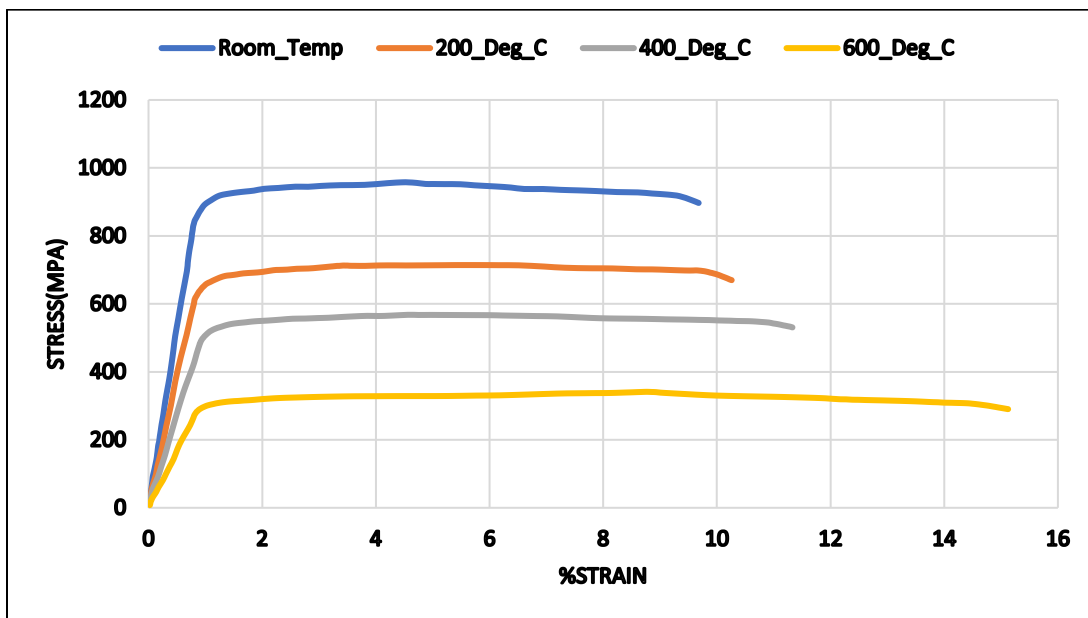


Figure 3. 3: Stress vs Strain curve for tensile testing sample



Figure 3. 4: Fracture of tensile testing sample at room temperature

As the temperature rose to 200°C, the material weakened. The yield stress dropped to 694 MPa, and the UTS decreased to 714 MPa. Despite this, the material still showed ductile behavior, fracturing at a slightly higher elongation of 10.2%.

Heating the material to 400°C resulted in a significant decrease in its mechanical properties. The yield strength fell to 550 MPa, and the UTS dropped further to 567 MPa, indicating a notable reduction in its ability to withstand deformation and failure.

At the highest tested temperature, 600°C, the material exhibited a drastic decline in both yield stress and UTS. The yield stress decreased to 320 MPa, and the UTS dropped critically low to 340 MPa. Despite this weakened state, the material showed significant elongation, up to 15%, before fracturing. The values are tabulated in table3.1.



Figure 3. 5: Fracture of tensile testing sample at elevated temperatures

Table 3.1: Properties obtained from Tensile testing samples at elevated temperatures.

S. NO	Temperature (C)	Tensile strength (MPa)	Yield strength. (MPa)	Young's Modulus (GPa)	%age Elongation
1	RT	952	938	108	9.6
2	200	714	694	74	10.2
3	400	567	550	55	11.5
4	600	340	320	32	15

3.4 3 Point bending test Results:

The load vs deflection curve obtained from the 3-point bending test was used to calculate the bending strength, flexural modulus, and critical stress intensity factor. The load vs deflection curve for 3 different tested samples is shown in figure 3.6.

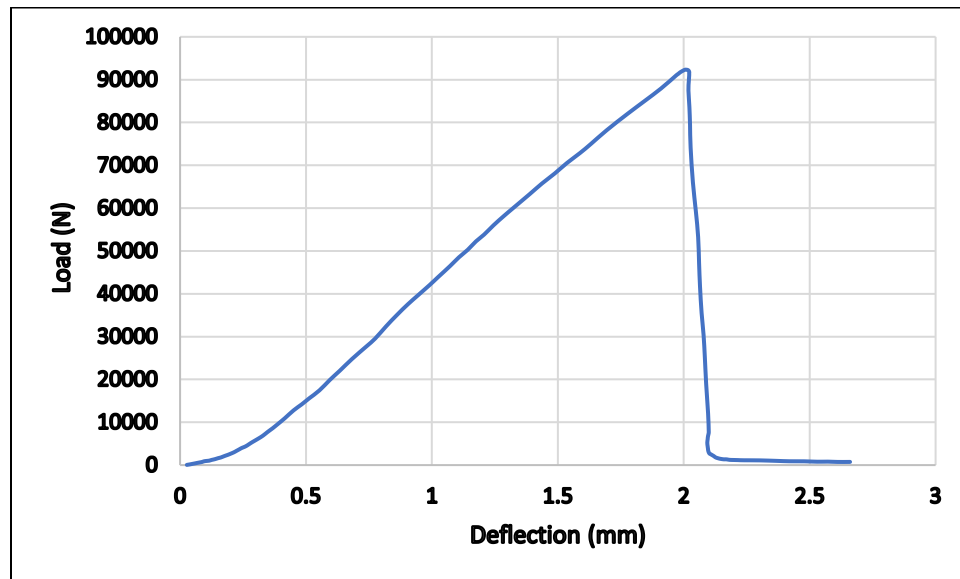


Figure 3. 6: load vs deflection curve for tensile testing sample

In the conducted test, the deformation behavior of the material was observed through a stress-strain curve. Initially, the curve began from the origin, signifying the absence of any initial load. As the load was applied linearly, the deflection increased proportionally, in accordance with Hooke's Law, which states that stress is directly proportional to strain. During this Elastic Deformation Phase, the material displayed elasticity, allowing it to deform under load while retaining the capability to revert to its original shape once the load was removed.

As the applied load continued to increase, the curve reached its peak at approximately 2 mm deflection and around 90,000 N load, marking the Ultimate Strength or Peak Point. This peak point indicated the material's maximum load-bearing capacity before it underwent failure.

Subsequently, as the load surpassed this peak, the curve sharply descended, indicating the onset of Plastic Deformation or the Failure Phase. At this stage, the material exceeded its yield strength and lost its ability to return to its original shape even when the load was released.

Finally, the curve flattened out at the bottom, representing the point of Complete Failure. The area under the curve up to the peak was identified as the energy absorbed during testing, which was crucial for assessing the material's toughness.



Figure 3. 7: Breakage of fracture toughness test sample

Calculation

Load at fracture = 93.98kN

Max deflection = 2.09 mm

$$\text{Bending Stress} = \sigma_b = \frac{MC}{I} = \frac{3FL}{2bd^2} = \frac{3 \cdot 93980 \cdot 100}{2 \cdot 25 \cdot 25^2} = 902 \text{MPa}$$

$$\text{Bending Strain} = \epsilon_b = \frac{6Dd}{L^2} = \frac{6 \cdot 2.09 \cdot 25}{100^2} = 0.031$$

$$\text{Flexural Modulus} = \frac{\sigma_b}{\epsilon_b} = \frac{902}{0.031} = 28.77 \text{GPa}$$

$$\text{Critical Stress intensity factor} = K_{IC} = \frac{F \cdot L}{B \cdot W^{\frac{3}{2}}} * f\left(\frac{a}{W}\right) = \frac{93.98 \cdot 10}{2.5 \cdot 2.5^{\frac{3}{2}}} * 2.66 = 89.44 \text{MPa} \cdot \text{m}^{\frac{1}{2}}$$

Whereas:

F = Max load applied

L = Span length

b = Sample thickness

w = Sample height

D = Max deflection

B = Sample thickness (As per testing standard E399).

Table 3.2: 3-point bending test results

S. No	Results	Values
1	Load at fracture	93.98 KN
2	Maximum deflection	2.09 mm
3	Bending strength	902MPa
4	Flexural modulus	28.77GPa
5	Critical stress intensity factor	89.44MPa·m ^{1/2}

3.5 Rockwell Hardness test Result:

The hardness test for the 3D printed Ti6Al4V was performed, adhering to the ASTM E 10 standard. This procedure utilized a Rockwell hardness tester with a diamond cone indenter, specifically selecting the type C scale, which is appropriate for medium hard materials like Ti6Al4V. Initially, a minor load of 98N was applied to the specimen measuring 25x25x4 mm to ensure contact with the indenter. Subsequently, a major load of 150 kg was briefly imposed and then removed, resulting in a permanent indentation on the specimen.

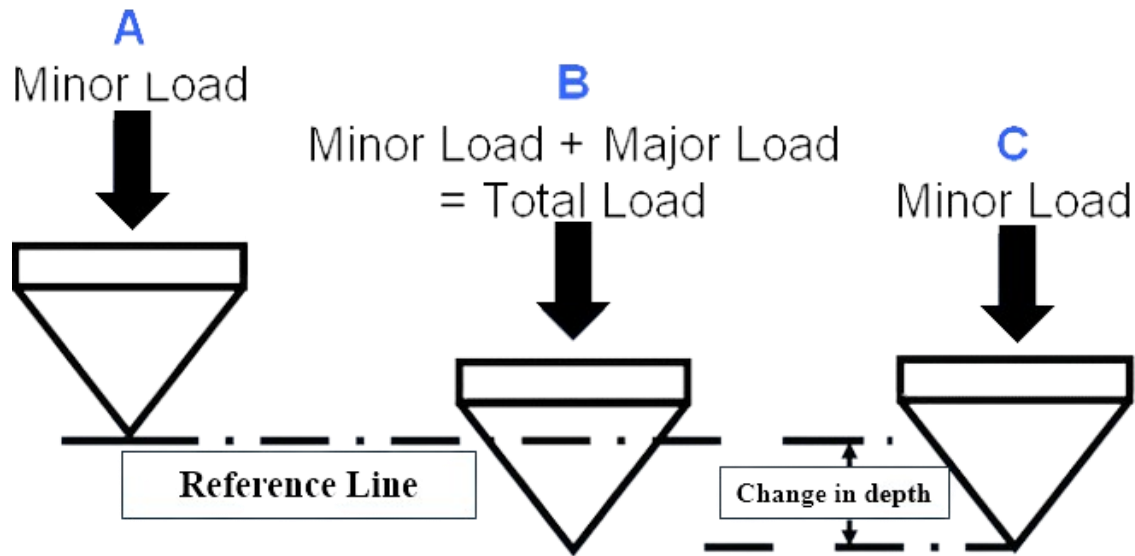


Figure 3. 8: Rockwell hardness testing

The depth of this indentation was then used to calculate the hardness value using the formula $HRC = 100 - (\text{change in depth}(\text{mm}) / 0.002)$. The final hardness value determined for the Ti6Al4V, produced with selective laser melting technique, was established at 37 HRC.

The Figure illustrates the Rockwell hardness testing process in three stages. The initial stage shows the indenter poised above the material's surface, ready to apply the minor load. The second stage depicts the application of both minor and major loads, exerting total pressure on the material. In the final stage, the major load is retracted, maintaining only the minor load, and the change in depth due to the indentation is evident. A reference line across all stages marks the original level of the material's surface.

3.6 Thermal conductivity test Results:

Thermal conductivity increases with an increase in temperature as shown in the graph. It shows an almost linear relationship. Thermal conductivity increases with the temperature due to the following reasons.

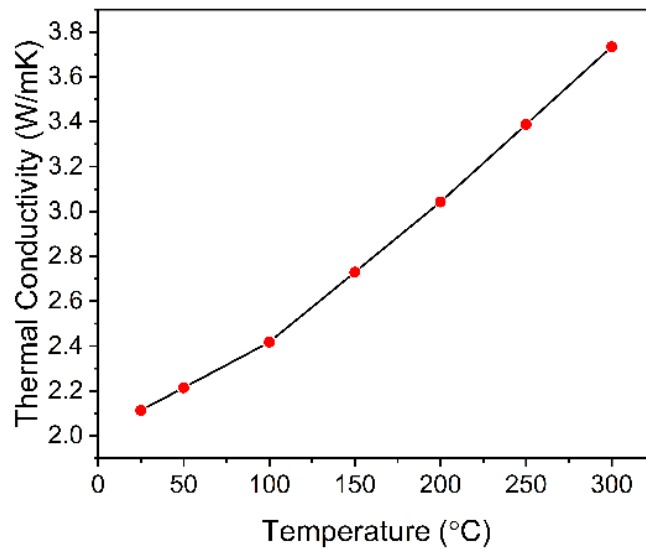


Figure 3. 9: Thermal conductivity vs Temperature plot

- **Lattice Vibrations:** At higher temperatures, lattice vibrations become more vigorous. This increased vibrational energy facilitates better energy transfer through the material, leading to higher thermal conductivity.
- **Free Electrons:** As temperature rises, free electrons gain more kinetic energy. These electrons contribute significantly to heat conduction. Their enhanced mobility results in higher thermal conductivity.
- **Microstructure Changes:** The alloy's microstructure evolves with heating. Certain phases may become more accessible or efficient pathways for heat conduction.
- **Crystal Defects:** Dislocations, vacancies, and grain boundaries influence thermal conductivity. At elevated temperatures, these defects can impact heat flow.
- **Alloy Composition:** Ti6Al4V alloy's specific composition affects its thermal properties. The balance of titanium, aluminum, and vanadium influences how heat is conducted.
- **Grain Size:** Finer grain sizes often lead to higher thermal conductivity due to reduced phonon scattering.

3.7 Thermal coefficient of expansion Test Results:

Coefficient of thermal expansion increases with increase in temperature as shown in graph.

Coefficient of thermal expansion increases due to the following reasons.

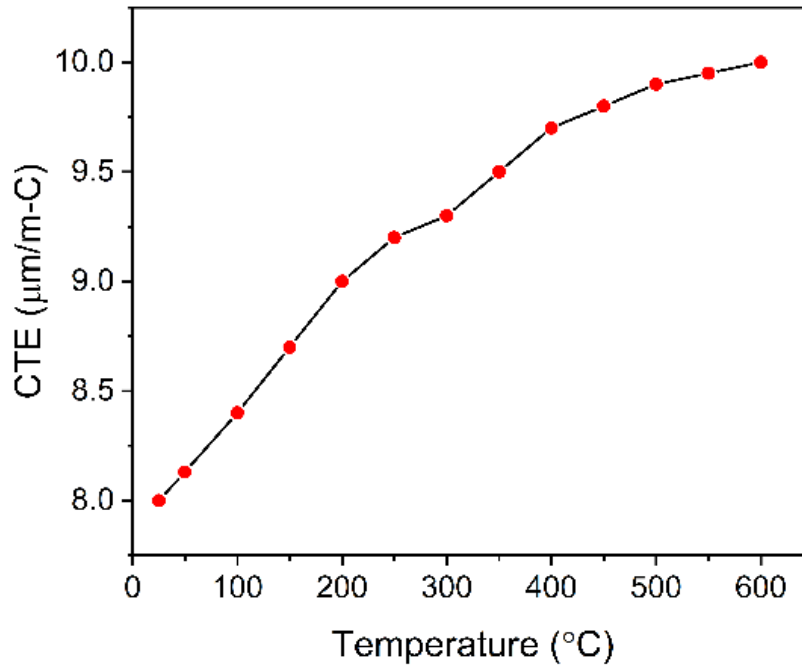


Figure 3. 10: CTE vs Temperature Plot

In CTE test, the behavior of the material's Coefficient of Thermal Expansion (CTE) was examined across various temperature ranges using a stress-strain curve. At higher temperatures, atomic vibrations became more pronounced, with increased energy leading to greater spacing between atoms, resulting in expansion. This phenomenon can be attributed to thermal excitation, where rising temperatures provided atoms with kinetic energy, promoting lattice vibrations, and pushing neighboring atoms apart.

Furthermore, changes in the material's crystal structure or phase transitions were observed to influence its CTE. For instance, in the case of Ti6Al4V, phase transformations occurred with variations in temperature, affecting its CTE. Additionally, microstructural effects such as grain boundaries, dislocations, and defects were found to play a significant role in influencing the CTE

of the material. These microstructural features evolved with temperature, consequently impacting the material's expansion behavior.

Moreover, the material's anisotropic behavior also contributed to its CTE variation. Some materials exhibit different expansion rates along various crystallographic directions, and Ti6Al4V's anisotropic behavior was observed to be a contributing factor in its CTE variability.

3.8 Specific heat capacity Test Results:

Specific heat obtained from DSC at different temperatures are plotted as shown in graph.

As temperature increases from left to right, the specific heat capacity initially rises.

It reaches a plateau around 200°C and then decreases.

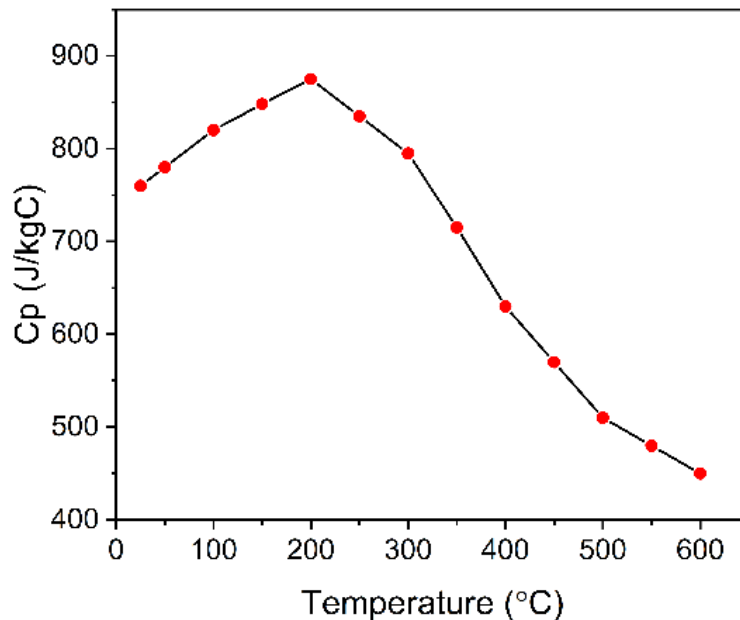


Figure 3. 11: Specific heat vs Temperature Plot

In the above conducted test, the specific heat behavior of the material was analyzed across a range of temperatures using a stress-strain curve. Initially, up to approximately 200°C, there was an increase in specific heat. This rise can be attributed to the material absorbing energy, which serves to relieve internal stresses induced during Selective Laser Melting (SLM) processing. Additionally,

other phenomena such as phase changes or lattice vibrations may have contributed to this initial increase.

Subsequently, between 200°C and 400°C, the specific heat remained relatively stable, forming a plateau. During this phase, no significant phase changes were observed, indicating consistent behavior in terms of energy absorption.

However, beyond 400°C, a decrease in specific heat was noted. Several factors contributed to this decline, including phase transformations where Ti6Al4V underwent an α to β phase transformation at elevated temperatures. Furthermore, increased atomic vibrations at higher temperatures led to a reduction in specific heat. Additionally, various thermal effects, such as changes in crystal structure, defects, and anisotropy, also played a role in this observed decrease.

3.9 Numerical Simulations:

The mass of the initial control surface is reduced by 53% maintaining its Cg in original location. Finite Element Analysis is used for comparison between initial control surface with standard Ti6Al4V properties and Final ribbed structure design with 3D printed properties. Static Structural Module of Ansys is used for this purpose. The mechanical and thermal properties of 3D printed Ti6Al4V alloy using selective laser melting method is assigned to the designed control surface and is analyzed in Ansys mechanical against the flight loading condition. Also, the initial design of control surface is analyzed with the standard mechanical and thermal properties of standard Ti6Al4V alloy.

Hex Dominant method is applied with body sizing of 5mm to have a fine mesh with total nodes = 46000 and element = 31000.

3.9.1 Boundary Conditions:

Control surface is constrained from holes in all three directions as it is attached to main body through bolts fixing it in three axes. Loads are applied accordingly in axial direction and normal to the surface.

3.9.2 Results:

The Von- mises stresses and deformation plots are shown in figures below for both cases.

3.9.2.1 Von-Mises stress:

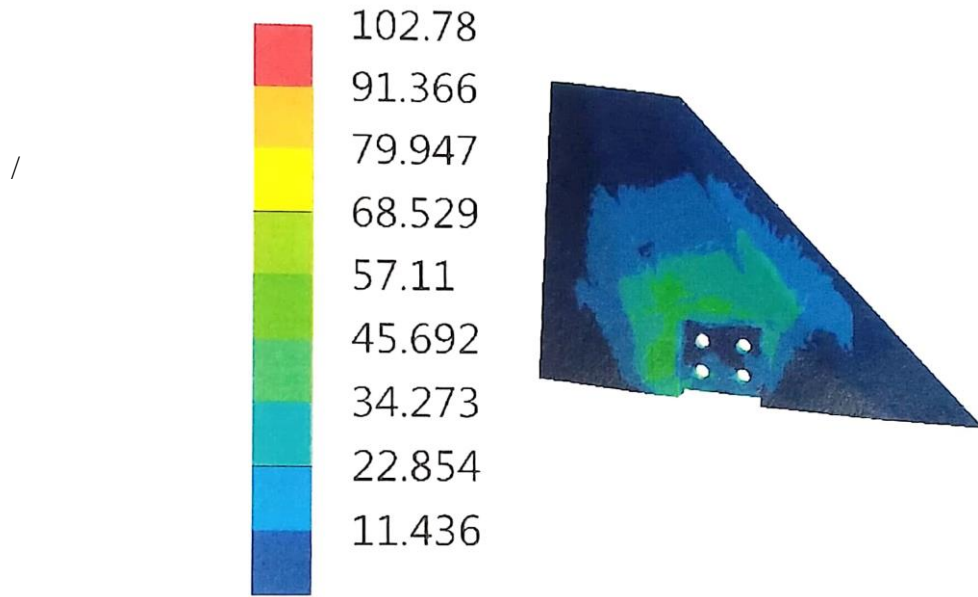


Figure 3. 12: Von-Mises Stress (MPa) in initial solid control Surface

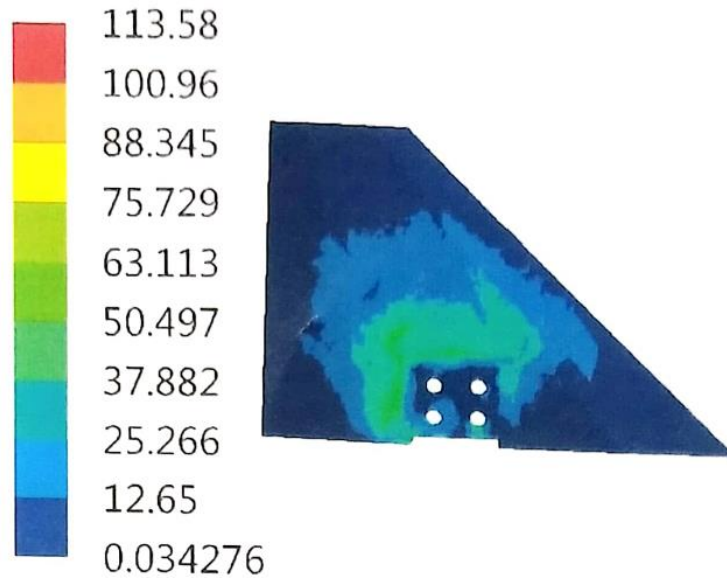


Figure 3. 13: Von-Mises Stress (MPa) with test properties

3.9.2.2 Total Deformation:

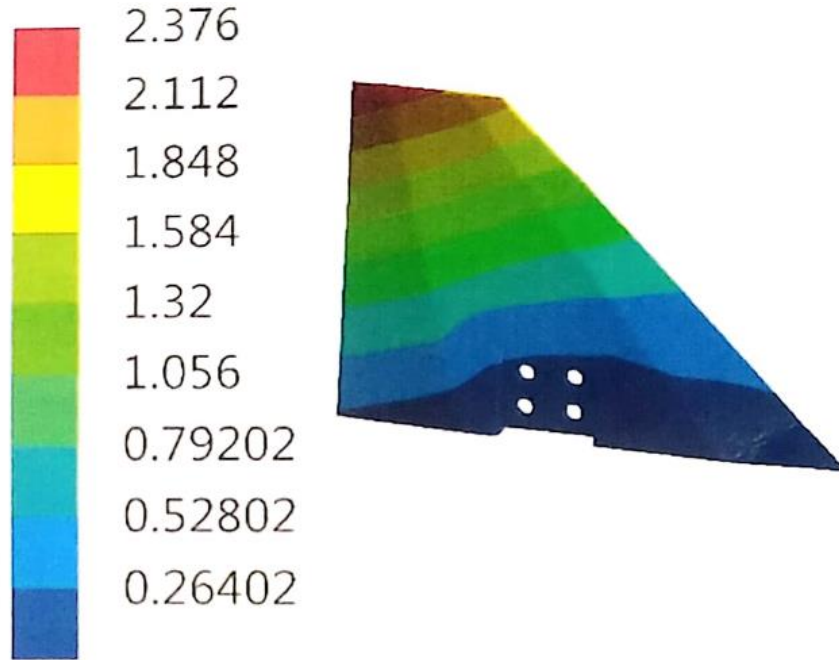


Figure 3. 14: Total Deformation (mm) in initial solid control Surface

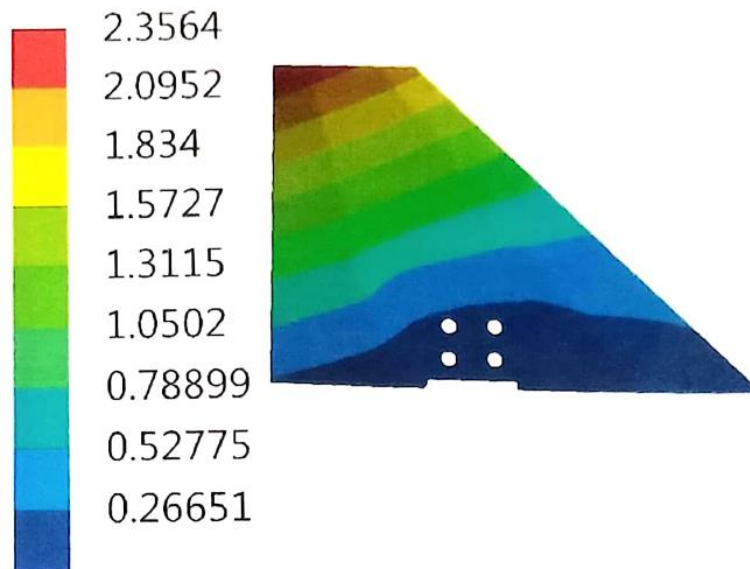


Figure 3. 15: Total Deformation (mm) with test properties

3.9.3 Conclusion

The FEA results are comparable, and the design has considerable factor of safety when compared with strength of material for both standard and tested properties. The percentage difference in von-mises stress and deformation for both initial with standard and Final ribbed structure with tested properties are given in table below.

Table 3.3: comparison of FEA results of initial solid design and final optimized ribbed structure design

S. No	Solution Results	Initial Design (solid design)	Final Design (ribbed structure design)	%age difference
1	Von-Mises stress (MPa)	102.78	113.58	9.6%
2	Total deformation (mm)	2.376	2.3564	0.8%

CHAPTER 4: DISCUSSION

The results obtained from the mechanical and thermal testing of selective laser melted Ti6Al4V are compared with the conventional manufactured Ti6Al4V alloy sheet. The values of Ti6Al4V sheets are taken from military standard MIL-HDBK-5J. All testing results are compared and discussed one by one:

4.1 Comparison between Tensile strengths of Ti6Al4v 3D printed Samples and

Conventional manufactured Ti6Al4v sheet:

Tensile strength values of Ti6Al4V sheet at different temperatures are taken from figure1. Tensile strength of Ti6Al4V decreases with increase in temperature. The figure shows percentage of room temperature strength with temperature variation. Percentage elongation of Ti6Al4V is shown in figure2. These values are compared in table4.1.

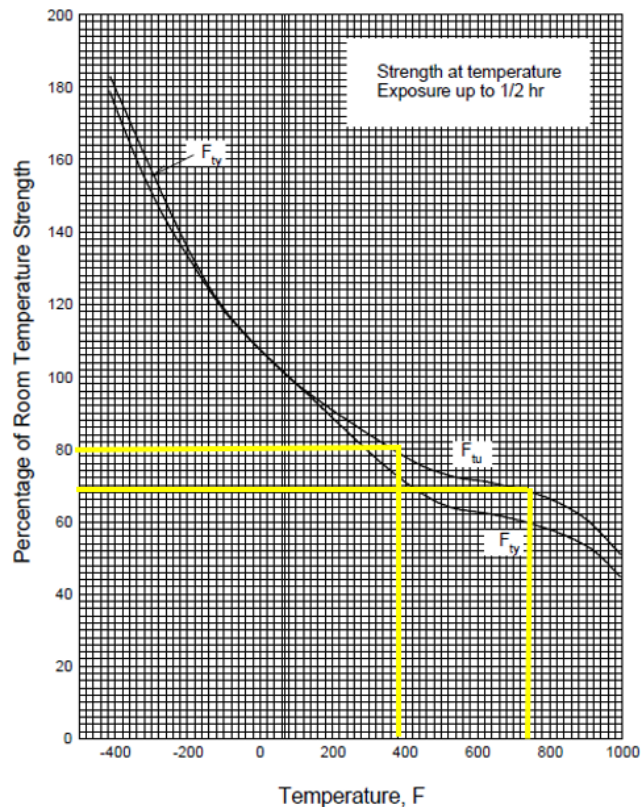


Figure 4. 1: Percentage of Room Temperature strength vs Temperature for Ti6Al4V sheet at different Temperature

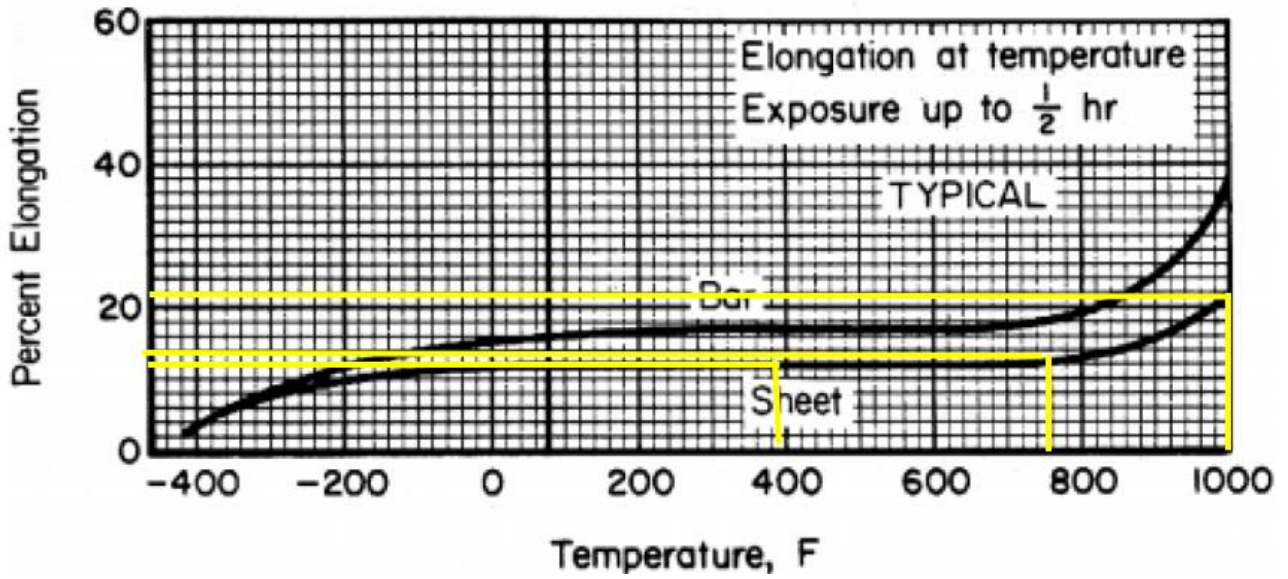


Figure 4. 2: Percent Elongation vs Temperature for Ti6Al4V sheet at different Temperature

Table 4.1: Comparison of tensile strength of 3D printed Tested samples of Ti6Al4V and standard properties of Ti6Al4V.

S. NO	Temperature (C)	Yield strength. (MPa)	Young`s Modulus (GPa)	%age Elongation	Tensile strength (MPa)	Tensile strength of Ti6Al4V sheet(MPa)	%age diff in strength
1	RT	938	108	9.6	952	935	1.8
2	200	694	74	10.2	714	730	2.2
3	400	550	55	11.5	580	640	9.3
4	600	320	32	15	340	NA	---

The Values of yield strength, young`s Modulus, tensile strength and fracture toughness are at par with values available in standard (HDBK-5J) for conventional manufactured parts, however breaking of tensile samples shows relatively less necking. %age elongation of 3D Samples are less than the traditional manufacturing metals as it shows a bit brittle behavior.

4.2 Comparison between thermal conductivity of Ti6Al4v 3D printed Samples and

Conventional manufactured Ti6Al4v sheet:

Values of thermal conductivity of Ti6Al4V sheets are obtained from the figure below. The thermal conductivity increases with an increase in temperature. Discrepancy in thermal conductivity between **selective laser melted (SLM) samples** and **Ti6Al4V sheets** are attributed to several factors discussed below:

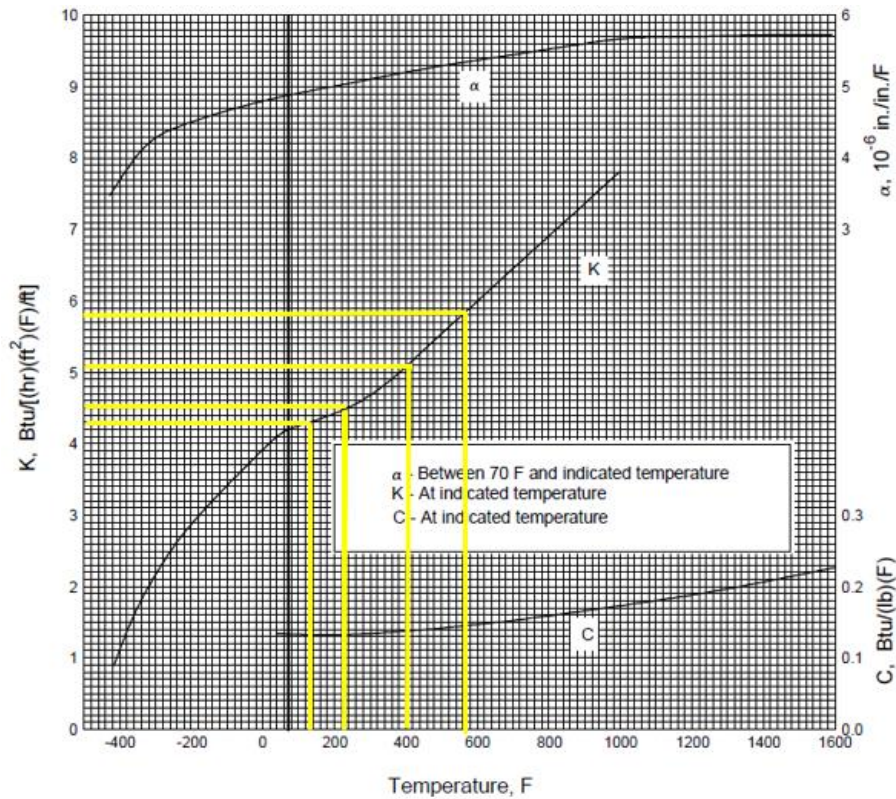


Figure 4. 3: Thermal Conductivity vs Temperature for Ti6Al4V sheet at different Temperature

Table 4.2: Comparison of thermal conductivity of 3D printed Tested samples of Ti6Al4V and standard properties of Ti6Al4V sheet.

S. No	Property	Temperature	Measured Values	MIL-HDBK-J
1	Thermal conductivity W/m k	RT	2.11	7.4
		100	2.41	7.8
		200	3.04	8.65
		300	3.73	9.7

➤ Microstructure Differences:

- SLMed samples have a distinct microstructure due to the layer-by-layer additive manufacturing process. Rapid solidification during SLM results in finer grain structures, hindering heat transfer.
- Sheets, produced through conventional methods, have larger grain sizes and better thermal conductivity.

➤ Anisotropy:

- SLMed samples are **anisotropic**, with properties varying by direction. Building orientation during printing affects thermal conductivity.
- As the polar angle of the specimen increases from 0° to 90°, thermal conductivity tends to increase.

➤ Process Variables:

- **Laser scan speed** and **hatch spacing** impact microstructure. Higher speeds and wider spacing reduce thermal conductivity.

- Adjusting these parameters affects heat flow paths within the material.
- Cellular Microstructure:
 - SLMed samples' solidified melt pool consists of cells with an **Al matrix** and a surrounding **Si-rich area**.
 - Variations in cell shape, size, and composition influence thermal conductivity.
- Martensite Formation:
 - Rapid cooling during SLM promotes **martensite**, a brittle phase. Sheets have a more ductile ferrite phase.
 - Brittle phases impede heat transfer.
- Powder Porosity:
 - **Packing density** affects powder porosity, a key parameter for thermal conductivity.
 - SLMed samples may have higher porosity, reducing overall thermal conductivity.

In summary, SLM introduces microstructural variations, anisotropy, and altered material properties, leading to lower thermal conductivity compared to traditional sheets.

4.3 Comparison between coefficient of thermal expansion of Ti6Al4v 3D printed Samples and Conventional manufactured Ti6Al4v sheet

coefficient of thermal expansion of Ti6Al4V sheet is taken from figure4.4. The values of CTE obtained from the testing of selective laser melted samples is compared with the ti6al4v sheet values from MIL-HDBK 5J.

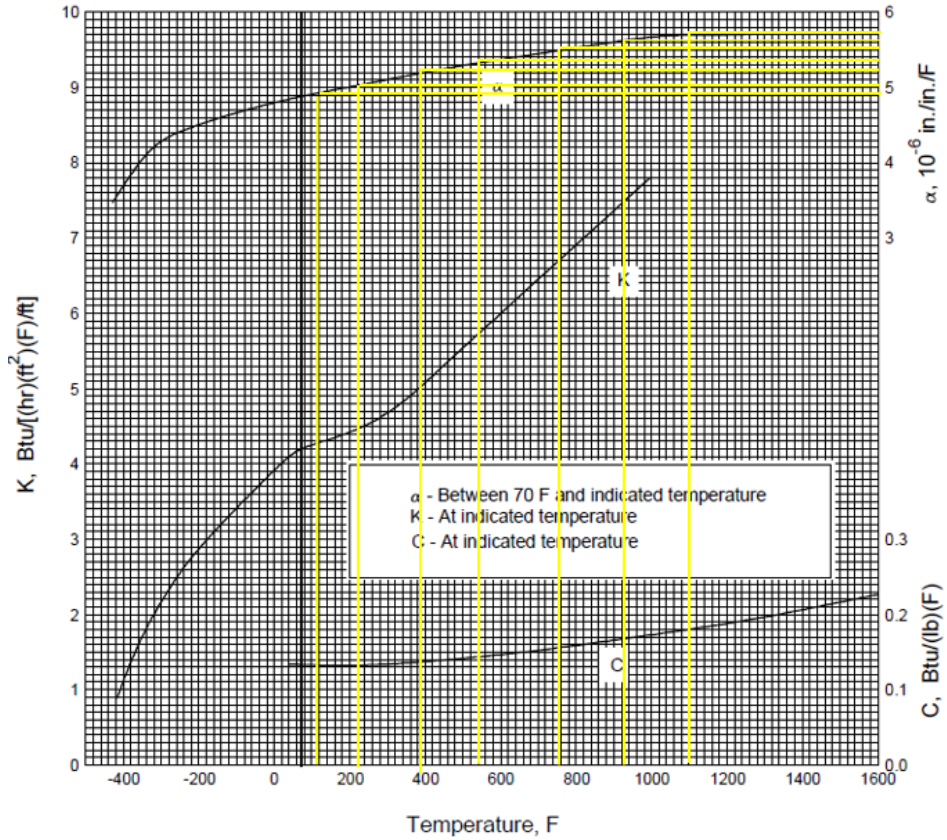


Figure 4. 4: CTE vs Temperature for Ti6Al4V sheet at different Temperature

Table 4.3: Comparison of CTE of 3D printed Tested samples of Ti6Al4V and standard properties of Ti6Al4V sheet.

S. No.	Properties	Temperature	Measured Values	HDBK	%age difference
1	CTE $\mu\text{m}\backslash\text{m}$ (10^{-6})	RT	8	8.8	10
		100	8.4	9	7.1
		200	9	9.4	4.4
		300	9.3	9.7	4.3
		400	9.7	9.9	2.06
		500	9.9	10.1	2.02
		600	10	10.3	3

The measured value of CTE shows a little variation at low temperatures, however at elevated temperatures, it is within range.

➤ Vibrational Origin:

- As the temperature increases, the **kinetic energy** of atoms and molecules within the material also rises.
- These heated particles vibrate more vigorously and occupy greater average distances from each other.
- Consequently, the material **expands** due to this increased vibrational motion.

➤ Atomic Bonding and Interactions:

- At higher temperatures, the **interatomic forces** weaken.
- Weaker bonds allow for more **thermal expansion** as atoms and ions move apart.
- The balance between cohesive forces and thermal conditions determines the overall expansion.

➤ Anharmonicity:

- The **anharmonicity** of atomic vibrations plays a role.
- At elevated temperatures, the harmonic approximation (simple harmonic motion) breaks down.
- Anharmonic effects lead to deviations from linear expansion behavior.

➤ Lattice Dynamics:

- The **lattice vibrations** within the crystal structure contribute to thermal expansion.
- As temperature increases, lattice vibrations become more pronounced, leading to expansion.

The above tested mechanical properties verified that the performance is satisfactory and equivalent to the traditional manufacturing of bulk Ti6Al4V alloy. SLM is new additive

manufacturing technology and this study suggested that SLM technology is best alternate to produce products for different applications in aerospace with light weight, same strength as conventional manufactured parts, less leading time, and high cost effective.

4.4 Comparison between Specific heat of Ti6Al4v 3D printed Samples and Conventional manufactured Ti6Al4v sheet:

Specific heat of Ti6Al4V sheet is shown in figure 3. Specific heat also increases with increase in temperature for Ti6Al4V sheets but for Selective laser melted Ti6Al4V alloy it shows a different trend. The **specific heat** behavior of **selective laser melted (SLM) Ti6Al4V samples** differing from that of standard Ti6Al4V attributed to several factors discussed below.

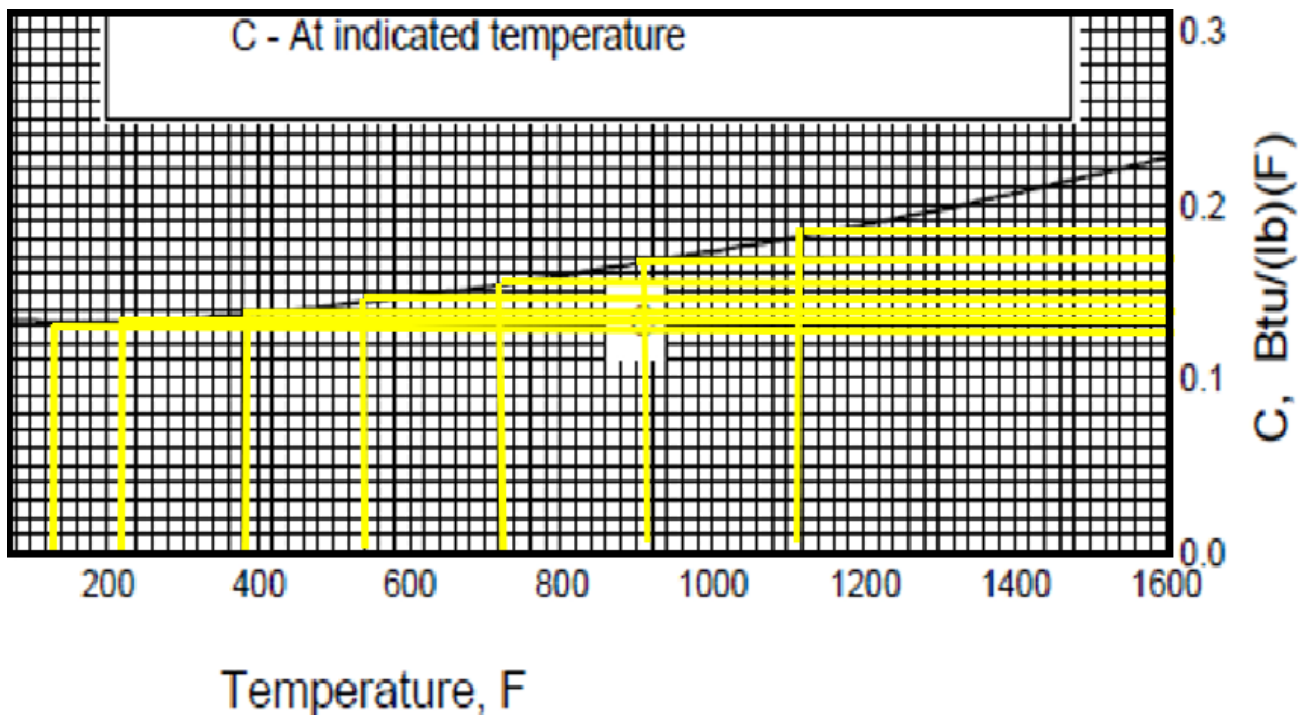


Figure 4. 5: Specific heat vs Temperature for Ti6Al4V sheet at different Temperature

Table 4.4: Comparison of Specific heat of 3D printed Tested samples of Ti6Al4V and standard properties of Ti6Al4V sheet.

S. No	Properties	Temperature	Measured Values	MIL-HDBK-J
1	Cp J/kg C	RT	760	565
		100	875	565
		200	925	586
		300	795	607
		400	630	649
		500	510	712
		600	450	754

Initial Increase in Cp:

- As the temperature rises, the **vibrational modes** of atoms and lattice structures become more active.
- Initially, this leads to a **gradual rise in specific heat** as the material absorbs more energy due to increased internal degrees of freedom (such as vibrations).

Peak and Transition:

- At a certain temperature (often referred to as the **Debye temperature**), the material reaches its maximum specific heat capacity.
- Beyond this point, additional energy input does not significantly increase vibrational modes or internal energy.

Phonon Scattering and Anharmonicity:

- Further temperature increase results in **phonon scattering** becoming more pronounced.
- Phonons are quantized vibrational modes in the crystal lattice.

- Anharmonic interactions lead to **phonon-phonon scattering**, reducing overall specific heat capacity.
- Lattice vibrations become less efficient at carrying heat energy.

Defects and Dislocations:

- Elevated temperatures involve **defects, dislocations, and grain boundaries**.
- These hinder phonon flow and reduce C_p .
- Dislocations act as **phonon traps**, absorbing energy and decreasing overall heat capacity.

Phase Transitions:

- If the material undergoes **phase transitions** (such as melting, recrystallization, or phase changes), the specific heat behavior changes abruptly.
- For example, during **solid-to-liquid transition** (melting), C_p differs significantly from the solid phase. The specific heat capacity (C_p) behavior of Ti6Al4V samples produced through Selective Laser Melting (SLM) exhibits an interesting trend with increasing temperature:

Electronic Contributions:

- At very high temperatures, electronic contributions to specific heat become significant.
- Electronic specific heat capacity depends on **density of states** and **Fermi energy**.
- Metals exhibit a **linear increase** in electronic specific heat with temperature.

In summary, the initial rise in specific heat capacity is due to increased vibrational modes, but subsequent factors such as phonon scattering, defects, and phase transitions lead to the observed decline beyond a certain temperature. The complex interplay of lattice dynamics, electronic behavior, and material structure determines Ti6Al4V alloy's specific heat behavior with temperature.

Table 4.5: Comparison of 3D printed Tested Properties of Ti6Al4V and standard properties of Ti6Al4V.

S. N0	Properties	Temperature	Testing values	Mil-HDBK-5J
1	Tensile Strength (MPa)	RT	952	935
		200C	714	730
		400C	567	643
		600C	340	NA
2	Yield Strength (MPa)	RT	938	869
3	Young`s Modulus (GPa)	RT	108	116
4	%age Elongation	RT	9.2 to 15	10 up to 400C & 20 at 600C
5	Hardness “HRC”	RT	37	35
6	Fracture Toughness (MPa.m ^{1/2})	RT	89.44	115
7	Thermal conductivity W/m k	RT	2.11	7.4
		100	2.41	7.8
		200	3.04	8.65
		300	3.73	9.7
8	CTE μm\m (10 ⁻⁶)	RT	8	8.8
		100	8.4	9
		200	9	9.4
		300	9.3	9.7
		400	9.7	9.9
		500	9.9	10.1
		600	10	10.3
9	Cp J/kg C	RT	760	565
		100	875	565
		200	925	586
		300	795	607
		400	630	649
		500	510	712
		600	450	754

Values of yield strength, young's Modulus, tensile strength and fracture toughness are at par with values available in standard (HDBK-5J) for conventional manufactured parts, however breaking of tensile samples shows relatively less necking. %age elongation of 3D Samples are less than the traditional manufacturing metals as it shows a bit brittle behavior. Also, CTE values have high variations at RT, however at elevated temperature it is within range. Furthermore, thermal conductivity is approximately 6 times lesser than standard values. Specific heat trend at higher temperatures is in reverse order as compared to standard.

CHAPTER#05 CONCLUSION

Control surface of an aero vehicle vertical often referred to as the tail fin, is a fixed vertical surface located at the rear of an aircraft. It is very crucial component of an aircraft's empennage (tail section) and plays a vital role in maintaining the aircraft's stability and control during flight. The primary purpose of the vertical stabilizer is to provide control, stability, and trim in the yaw axis (also known as directional stability). It compensates for moments generated by asymmetry in thrust or drag, allowing the aircraft to maintain a straight course during flight.

This work illustrates the mass reduction of control surface manufactured from solid block using conventional manufacturing technique. Design was finalized after successive iterations of topology optimization keeping in view centre of gravity and selective laser melting machine manufacturing constraints. Initially two pocket was introduced in the structure maintaining Cg at X- location but mass reduction was about 18%. After that honeycomb structure was introduced for further mass reduction, but the idea was dropped due to manufacturing constraints the metal powder will be trapped in honeycomb cells. The mass reduction in this case was 42%. At Final design rib structure were used to provide extra strength in bending, and pockets were introduced along with the slots at each pocket exit location for removal of powdered metal from inside the body. The mass reduction for the final case was 53%.

For material characterization, samples were printed by selective laser melting technique by FARSOON machine with laser power of 280W, scanning speed 1200mm/s, layer thickness 40mm and hatch distance of 80mm. Five samples were printed and tested on universal testing machine with strain rate 2mm/min according to ASTM E8M-4 standard at room temperature and GB 228 standard at 200,400 & 600C respectively. At room temperature (RT), the material exhibited an Ultimate Tensile Strength (UTS) of 952 MPa and fractured upon reaching the maximum stress, with an elongation of 9.2%. When subjected to 200°C, there was a 25% reduction in strength; the Yield Stress dropped to 694 MPa and UTS decreased to 714 MPa, with fracture occurring at 10.2% elongation. At 400°C, a significant decrease in strength was observed with the Yield Stress at 550 MPa and UTS at 567 MPa, marking a 40% reduction in strength. Further, at 600°C, the material demonstrated minimal Yield Stress of 320 MPa and a critically low UTS of 340 MPa, with elongation extending up to 15%. This represented a substantial 64% reduction in strength.

Three-point bend testing was performed on 03 printed samples according to ASTM E 399 to measure fracture toughness at room temperature. The load at fracture was determined to be 93.98 KN, while the maximum deflection observed was 2.09 mm. The material demonstrated a bending stress of 902 MPa and a corresponding bending strain of 0.031. Additionally, the Flexural Modulus was calculated to be 28.77 GPa. An important parameter, the Critical Stress Intensity Factor, was measured at 89.44 MPa·m^{1/2}. The hardness of sample was measured by Rockwell hardness tester with cone type diamond indenter according to ASTM E 10. The measured value for the tested sample was 37HRC. The thermal conductivity of a 3D printed sample was assessed using the ASTM E 1530 standard and a Guarded heat flow meter. The steady-state through-thickness temperatures were recorded at room temperature (RT), 100°C, 200°C, and 300°C. At room temperature (RT), the thermal conductivity was 2.11 W/m·K, which increased to 2.41 W/m·K at 100°C. Subsequently, at 200°C, the thermal conductivity further rose to 3.04 W/m·K, and at 300°C, it reached its highest value of 3.73 W/m·K. The thermal coefficient of expansion (CTE) of 3D printed samples was assessed using ASTM E228 on a Dilatometer (DIL-402C) at various temperatures: room temperature (25°C), 100°C, 200°C, 300°C, 400°C, 500°C, and 600°C. The obtained Coefficient of Thermal Expansion (CTE) values for the material varied with temperature. At room temperature, the CTE was measured at 8 µm/m·°C. As the temperature increased, the CTE values also rose at 100°C, it increased to 8.4 µm/m·°C; at 200°C, it further rose to 9 µm/m·°C; at 300°C, it reached 9.3 µm/m·°C; at 400°C, it was 9.7 µm/m·°C; at 500°C, it was 9.9 µm/m·°C; and at 600°C, it reached 10 µm/m·°C. The specific heat capacity of Ti6Al4V powder was determined in accordance with ASTM E 1269 standards using a differential scanning calorimeter. Measurements were taken at various temperatures ranging from room temperature to 600°C. At 25°C, the specific heat capacity was recorded at 760 J/kg°C. As the temperature increased, there was an observed fluctuation in the specific heat capacity values: at 100°C, it rose to 820 J/kg°C; at 200°C, it increased further to 875 J/kg°C; and at 300°C, it decreased to 795 J/kg°C. Subsequently, at 400°C, a notable decrease was observed with a value of 630 J/kg°C. The specific heat capacity continued to decrease as the temperature rose to 500°C and 600°C, with values of 510 J/kg°C and 450 J/kg°C, respectively.

Finite Element Analysis is used for comparison between initial control surface with standard Ti6Al4V properties and Final ribbed structure design with 3D printed properties. Static Structural

Module of Ansys is used for this purpose. The mechanical and thermal properties of 3D printed Ti6Al4V alloy using selective laser melting method is assigned to the designed control surface and is analyzed in Ansys mechanical against the flight loading condition. Also, the initial design control surface is analyzed with the standard mechanical and thermal properties of standard Ti6Al4V alloy. The finite element analysis (FEA) results indicate that the design exhibits a significant factor of safety when compared to the material strength, both for standard and tested properties. Specifically, we observe the following percentage differences in von-Mises stress and deformation between the initial design (based on standard properties) and the final ribbed structure (using tested properties). A comparison between the initial design (based on standard properties) and final ribbed structure designs (using tested properties) reveals slight differences in the von-Mises stress and total deformation. Specifically, the von-Mises stress for the initial design was 102.78 MPa, whereas the final design registered a slightly higher value of 113.58 MPa, representing a 9.6% increase. In terms of total deformation, the initial design exhibited a deformation of 2.376 mm, whereas the final design showed a slightly reduced deformation of 2.3564 mm, indicating a 0.8% decrease.

The ribbed structure design was safe with a factor of safety greater than 8 and with mass reduction of 53% against the same flight loading conditions. The final designed control surface can be utilized without changing its X center of gravity with considerable factor of safety.

REFERENCES

- [1] B. D. Mahindru, P. Mahendru SRMGPC, T. Ganj, D. Mahindru α , and P. Mahendru σ , “Review of Rapid Prototyping-Technology for the Future,” *Type: Double Blind Peer Reviewed International Research Journal Publisher: Global Journals Inc*, vol. 13, 2013.
- [2] K. Wong, “K.V. Wong, A.Hernandez, ‘A Review of Additive Manufacturing,’ ISRN Mechanical Engineering, Vol 2012 (2012), Article ID 208760, 10 pages.,” *ISRN Mechanical Engineering*, vol. 2012, Aug. 2012, doi: 10.5402/2012/208760.
- [3] K. V. Wong and A. Hernandez, “A Review of Additive Manufacturing,” *ISRN Mechanical Engineering*, vol. 2012, pp. 1–10, Aug. 2012, doi: 10.5402/2012/208760.
- [4] “Wohlers Report 2011 - Wohlers Associates.” Accessed: Apr. 28, 2024. [Online]. Available: <https://wohlersassociates.com/product/wohlers-report-2011/>
- [5] W. E. Frazier, “Metal additive manufacturing: A review,” *J Mater Eng Perform*, vol. 23, no. 6, pp. 1917–1928, Apr. 2014, doi: 10.1007/S11665-014-0958-Z/FIGURES/9.
- [6] H. Bikas, P. Stavropoulos, and G. Chryssolouris, “Additive manufacturing methods and modeling approaches: A critical review,” *International Journal of Advanced Manufacturing Technology*, vol. 83, no. 1–4, pp. 389–405, Mar. 2016, doi: 10.1007/S00170-015-7576-2/METRICS.
- [7] S. Ford and M. Despeisse, “Additive manufacturing and sustainability: an exploratory study of the advantages and challenges,” *J Clean Prod*, vol. 137, pp. 1573–1587, Nov. 2016, doi: 10.1016/J.JCLEPRO.2016.04.150.
- [8] P. Stavropoulos and P. Foteinopoulos, “Modelling of additive manufacturing processes: A review and classification,” *Manuf Rev (Les Ulis)*, vol. 5, 2018, doi: 10.1051/MFREVIEW/2017014.
- [9] A. Haleem and M. Javaid, “Additive manufacturing applications in industry 4.0: A review,” *Journal of Industrial Integration and Management*, vol. 4, no. 4, Dec. 2019, doi: 10.1142/S2424862219300011.

- [10] M. Javaid and A. Haleem, "Using additive manufacturing applications for design and development of food and agricultural equipments," *International Journal of Materials and Product Technology*, vol. 58, p. 225, Jan. 2019, doi: 10.1504/IJMPT.2019.10018137.
- [11] C. Y. Yap *et al.*, "Review of selective laser melting: Materials and applications," *Appl Phys Rev*, vol. 2, no. 4, Dec. 2015, doi: 10.1063/1.4935926/123739.
- [12] T. D. Ngo, A. Kashani, G. Imbalzano, K. T. Q. Nguyen, and D. Hui, "Additive manufacturing (3D printing): A review of materials, methods, applications and challenges," *Compos B Eng*, vol. 143, pp. 172–196, Jun. 2018, doi: 10.1016/J.COMPOSITESB.2018.02.012.
- [13] I. Gibson, D. W. Rosen, and B. Stucker, "Additive manufacturing technologies: Rapid prototyping to direct digital manufacturing," *Additive Manufacturing Technologies: Rapid Prototyping to Direct Digital Manufacturing*, pp. 1–459, 2010, doi: 10.1007/978-1-4419-1120-9.
- [14] I. Gibson, D. Rosen, and B. Stucker, "Additive manufacturing technologies: 3D printing, rapid prototyping, and direct digital manufacturing, second edition," *Additive Manufacturing Technologies: 3D Printing, Rapid Prototyping, and Direct Digital Manufacturing, Second Edition*, pp. 1–498, Jan. 2015, doi: 10.1007/978-1-4939-2113-3.
- [15] S. Kumar, "Liquid Based Additive Layer Manufacturing," *Additive Manufacturing Processes*, pp. 131–145, 2020, doi: 10.1007/978-3-030-45089-2_8.
- [16] N. Tuncer and A. Bose, "Solid-State Metal Additive Manufacturing: A Review," *JOM*, vol. 72, no. 9, pp. 3090–3111, Sep. 2020, doi: 10.1007/s11837-020-04260-y.
- [17] S. Bremen, W. Meiners, and A. Diatlov, "Selective Laser Melting," *Laser Technik Journal*, vol. 9, no. 2, pp. 33–38, Apr. 2012, doi: 10.1002/LATJ.201290018.
- [18] W. Duan, M. Wu, J. Han, Y. Ma, and X. Miao, "Effect of layer thickness on the overhanging surface quality manufactured by selective laser melting," <https://doi.org/10.1177/09544062211052820>, vol. 236, no. 9, pp. 4818–4827, Dec. 2021, doi: 10.1177/09544062211052820.

- [19] I. Buj, A. Tejo Otero, and F. Fenollosa, “Development of AM Technologies for Metals in the Sector of Medical Implants,” *Metals (Basel)*, vol. 10, p. 686, May 2020, doi: 10.3390/met10050686.
- [20] B. D. Mahindru, P. Mahendru SRMGPC, T. Ganj, D. Mahindru α , and P. Mahendru σ , “Review of Rapid Prototyping-Technology for the Future,” *Type: Double Blind Peer Reviewed International Research Journal Publisher: Global Journals Inc*, vol. 13, 2013.
- [21] “What are the Advantages and Disadvantages of 3D Printing? - TWI.” Accessed: Apr. 28, 2024. [Online]. Available: <https://www.twi-global.com/technical-knowledge/faqs/what-is-3d-printing/pros-and-cons>
- [22] C. Y. Yap *et al.*, “Review of selective laser melting: Materials and applications,” *Appl Phys Rev*, vol. 2, no. 4, Dec. 2015, doi: 10.1063/1.4935926.
- [23] B. Dutta and F. H. (Sam) Froes, “The Additive Manufacturing (AM) of titanium alloys,” *Metal Powder Report*, vol. 72, no. 2, pp. 96–106, Mar. 2017, doi: 10.1016/j.mprp.2016.12.062.
- [24] “Titanium 3D Printing – The Ultimate Guide | All3DP Pro.” Accessed: May 27, 2024. [Online]. Available: https://all3dp.com/1/3d-printing-titanium-methods-printers-applications/#google_vignette
- [25] S. Liu and Y. C. Shin, “Additive manufacturing of Ti6Al4V alloy: A review,” *Mater Des*, vol. 164, Feb. 2019, doi: 10.1016/j.matdes.2018.107552.
- [26] T. S. Tshephe, S. O. Akinwamide, E. Olevsky, and P. A. Olubambi, “Additive manufacturing of titanium-based alloys- A review of methods, properties, challenges, and prospects,” *Heliyon*, vol. 8, no. 3. Elsevier Ltd, Mar. 01, 2022. doi: 10.1016/j.heliyon.2022.e09041.
- [27] J. C. Najmon, S. Raeisi, and A. Tovar, “Review of additive manufacturing technologies and applications in the aerospace industry,” *Additive Manufacturing for the Aerospace Industry*, pp. 7–31, Jan. 2019, doi: 10.1016/B978-0-12-814062-8.00002-9.
- [28] V. Mohanavel, K. S. Ashraff Ali, K. Ranganathan, J. Allen Jeffrey, M. M. Ravikumar, and S. Rajkumar, “The roles and applications of additive manufacturing in the aerospace and

- automobile sector,” *Mater Today Proc*, vol. 47, pp. 405–409, Jan. 2021, doi: 10.1016/J.MATPR.2021.04.596.
- [29] G. Shashi, M. A. R. Laskar, H. Biswas, and A. Saha, *A Brief Review of Additive Manufacturing with Applications*. 2017. doi: 10.6084/m9.figshare.12520667.
- [30] L. Verhoef, B. Budde, C. Chockalingam, B. Nodar, and A. van Wijk, “The effect of additive manufacturing on global energy demand: An assessment using a bottom-up approach,” *Energy Policy*, vol. 112, pp. 349–360, Jan. 2018, doi: 10.1016/j.enpol.2017.10.034.
- [31] A. Długosz and W. Klimek, *The optimal design of UAV wing structure*, vol. 1922. 2018. doi: 10.1063/1.5019124.
- [32] “Catalog of Airframe Products | PDF.” Accessed: Apr. 28, 2024. [Online]. Available: <https://www.slideshare.net/aviationaxis/airframe-products>
- [33] “12: The basic main components of a general aircraft[33] | Download Scientific Diagram.” Accessed: Apr. 26, 2024. [Online]. Available: https://www.researchgate.net/figure/The-basic-main-components-of-a-general-aircraft33_fig11_337657660
- [34] R. Liu, Z. Wang, T. Sparks, F. Liou, and J. Newkirk, “Aerospace applications of laser additive manufacturing,” *Laser Additive Manufacturing: Materials, Design, Technologies, and Applications*, pp. 351–371, Jan. 2017, doi: 10.1016/B978-0-08-100433-3.00013-0.
- [35] A. A. Shapiro *et al.*, “Additive Manufacturing for Aerospace Flight Applications,” <https://doi.org/10.2514/1.A33544>, vol. 53, no. 5, pp. 952–959, Jul. 2016, doi: 10.2514/1.A33544.
- [36] G. J. Schiller, “Additive manufacturing for Aerospace,” *IEEE Aerospace Conference Proceedings*, vol. 2015-June, Jun. 2015, doi: 10.1109/AERO.2015.7118958.
- [37] B. Müller and C. Fraunhofer IWU, *Fraunhofer Direct Digital Manufacturing Conference DDMC 2016. Conference Proceedings, March 2016, Berlin, Germany*.
- [38] J. D. López-Castro, A. Marchal, L. González, and J. Botana, “Topological optimization and manufacturing by Direct Metal Laser Sintering of an aeronautical part in 15-5PH stainless steel,” *Procedia Manuf*, vol. 13, pp. 818–824, 2017, doi: 10.1016/j.promfg.2017.09.121.

- [39] D. J. Munk, D. J. Auld, G. P. Steven, and G. A. Vio, "On the benefits of applying topology optimization to structural design of aircraft components," *Structural and Multidisciplinary Optimization*, vol. 60, no. 3, pp. 1245–1266, Sep. 2019, doi: 10.1007/s00158-019-02250-6.
- [40] A. Dagkolu, I. Gokdag, and O. Yilmaz, "Design and additive manufacturing of a fatigue-critical aerospace part using topology optimization and L-PBF process," in *Procedia Manufacturing*, Elsevier B.V., 2020, pp. 238–243. doi: 10.1016/j.promfg.2021.07.037.
- [41] Y. feng Liu, Y. ying Fan, X. feng Jiang, and D. A. Baur, "A customized fixation plate with novel structure designed by topological optimization for mandibular angle fracture based on finite element analysis," *Biomed Eng Online*, vol. 16, no. 1, Nov. 2017, doi: 10.1186/s12938-017-0422-z.
- [42] K. Cheng, Y. Liu, C. Yao, W. Zhao, and X. Xu, "A personalized mandibular implant with supporting and porous structures designed with topology optimization – a case study of canine," *Rapid Prototyp J*, vol. 25, no. 2, pp. 417–426, Feb. 2019, doi: 10.1108/RPJ-11-2017-0231.
- [43] R. Liu, Y. Chen, Y. Liu, Z. Yan, and Y. X. Wang, "Topological Design of a Trabecular Bone Structure with Morphology and Mechanics Control for Additive Manufacturing," *IEEE Access*, vol. 9, pp. 11123–11133, 2021, doi: 10.1109/ACCESS.2021.3050745.
- [44] O. Bittredge *et al.*, "Fabrication and Optimisation of Ti-6Al-4V Lattice-Structured Total Shoulder Implants Using Laser Additive Manufacturing," *Materials*, vol. 15, no. 9, May 2022, doi: 10.3390/ma15093095.
- [45] G. Vastola, G. Zhang, Q.-X. Pei, and Y.-W. Zhang, "Controlling of Residual Stress in Additive Manufacturing of Ti6Al4V by Finite Element Modeling," *Addit Manuf*, vol. 12, May 2016, doi: 10.1016/j.addma.2016.05.010.
- [46] P.-H. Li, W. G. Guo, W.-D. Huang, Y. Su, X. Lin, and K.-B. Yuan, "Thermomechanical response of 3D laser-deposited Ti-6Al-4V alloy over a wide range of strain rates and temperatures," *Materials Science and Engineering A*, vol. 647, pp. 34–42, Oct. 2015, doi: 10.1016/j.msea.2015.08.043.

- [47] S. Leuders *et al.*, “On the mechanical behaviour of titanium alloy TiAl6V4 manufactured by selective laser melting: Fatigue resistance and crack growth performance,” *Int J Fatigue*, vol. 48, pp. 300–307, 2013, doi: 10.1016/j.ijfatigue.2012.11.011.
- [48] K. Karolewska, B. Ligaj, M. Wirwicki, and G. Szala, “Strength analysis of Ti6Al4V titanium alloy produced by the use of additive manufacturing method under static load conditions,” *Journal of Materials Research and Technology*, vol. 9, no. 2, pp. 1365–1379, Mar. 2020, doi: 10.1016/j.jmrt.2019.11.063.
- [49] X. P. Ren *et al.*, “A comparative study on mechanical properties of Ti–6Al–4V alloy processed by additive manufacturing vs. traditional processing,” *Materials Science and Engineering: A*, vol. 817, Jun. 2021, doi: 10.1016/j.msea.2021.141384.
- [50] “Farsoon Metal 3D Printers: Overview | Top 3D Shop.” Accessed: Apr. 26, 2024. [Online]. Available: <https://top3dshop.com/blog/farsoon-metal-3d-printers-overview>
- [51] “High temperature tensile testing machine -.” Accessed: May 25, 2024. [Online]. Available: <https://www.cermacsrl.com/en/homepage/products-range/high-temperature-tensile-testing-machine/>
- [52] D. Scărlătescu, A. Modrea, and M. Stanciu, “Three-point Bend Test to Determine the Mechanical Behavior of the Tubes Used in Water Supply Networks,” *Procedia Manuf*, vol. 32, pp. 179–186, Jan. 2019, doi: 10.1016/j.promfg.2019.02.200.
- [53] P. Zhang and X. Wei, “Study on Flexural Strength and Flexural Modulus of Elasticity of Cement Stabilized Aggregate,” *Adv Mat Res*, vol. 287-290:, pp. 990–993, Jul. 2011, doi: 10.4028/www.scientific.net/AMR.287-290.990.
- [54] “pmc_4877153”.
- [55] S. R. Low, “NIST recommended practice guide :,” Gaithersburg, MD, 2001. doi: 10.6028/NBS.SP.960-5.
- [56] “Mitech MHRS-150 Digital Rockwell Hardness Tester-Mitech CO., Ltd.” Accessed: May 25, 2024. [Online]. Available: http://www.mitech-ndt.com/en/home/products_detail.php?flm=&lm=&lim=&id=694

- [57] “Guarded Heat Flow Meter GHFM-01 Laboratory Instrument.” Accessed: Apr. 26, 2024. [Online]. Available: <https://thermtest.com/ghfm-01>
- [58] “ASTM E1530 Guarded Heat Flow Meter Method.” Accessed: May 04, 2024. [Online]. Available: <https://www.azom.com/article.aspx?ArticleID=11518>
- [59] “TransitionPoint.” Accessed: May 25, 2024. [Online]. Available: <http://www.sscocom.tw/Orton/TransitionPoint.htm>
- [60] J. D. James, J. A. Spittle, S. G. R. Brown, and R. W. Evans, “A review of measurement techniques for the thermal expansion coefficient of metals and alloys at elevated temperatures,” 2001. [Online]. Available: <http://iopscience.iop.org/0957-0233/12/3/201>
- [61] J. Daw, J. Rempe, D. Knudson, K. Condie, and J. Crepeau, *Viability of Pushrod Dilatometry Techniques for High Temperature In-Pile Measurements*. 2008. doi: 10.2172/926333.
- [62] “DSC 3 Thermal Analysis System from METTLER TOLEDO : Get Quote, RFQ, Price or Buy.” Accessed: May 25, 2024. [Online]. Available: <https://www.news-medical.net/Thermal-Analysis-System-DSC-3-from-Mettler-Toledo>
- [63] “Differential Scanning Calorimetry -”. [Online]. Available: https://www.linseis.com/en/methods/differential-scanning-calorimetry-dsc/?gad_source=1&gclid=Cj0KCQjwudexBhDKARIsAI-GWYX19fIYdLQJ5XTyo71-U05axtYi0c9NRCfQBzjMGcf78nWJ3gupmqkaAq0lEALw_wcB